Antibody Mediated Diversification of Primary and Secondary Humoral Immune Responses

Dennis Schaefer-Babajew[1*†], Laurine Binet[1*], Gabriela S. Silva Santos[1], Chiara Ruprecht[1], Lachlan P. Deimel[1], Mohamed A. ElTanbouly[1], Dounia Gharrassi[1], Gabriella Lima dos Reis[1], Clara Uhe[1], Kai-Hui Yao[1], Brianna Hernandez[1], Parul Agrawal[2], Anna Gazumyan[1], Leonidas Stamatatos[2], Harald Hartweger[1 +], Michel C. Nussenzweig[1,3, +]

[1]Laboratory of Molecular Immunology, Rockefeller University; New York, NY, USA.

[2]Fred Hutchinson Cancer Center, Seattle, WA, USA

[3]Howard Hughes Medical Institute, The Rockefeller University; New York, NY, USA.

[†]Current address: Department of Internal Medicine, Yale School of Medicine, New Haven, CT, USA

*equal contribution

+equal contribution

Address correspondence to: nussen@rockefeller.edu or hhartweger@rockefeller.edu

Summary

Humoral immune responses diversify over time but whether secreted antibodies influence this process is unknown. Using antibody secretion-deficient mice this study shows a profound impact of secreted antibodies on the evolution of B cell diversity after vaccination.

Abstract

Humoral immune responses are characterized by increasing antibody affinity and diversity over time. Increased affinity is mediated by a combination of immunoglobulin gene somatic mutation and iterative cycles of selection in germinal centers. Less is understood about how diversity increases. Here we examine the role of antibody feedback in diversifying immune responses in mice that produce B cells that are incapable of secreting antibodies. To this end, we produced two strains of mice, one that expresses only membrane and secreted forms of IgM, and a second that produces only the membrane bound form of IgM. Analysis of primary and secondary immune responses show that antibody feedback significantly diversifies both primary and secondary immune responses even when antibodies are present at levels that are 10–30 fold lower than physiologic. The data have significant implication for sequential vaccination approaches aimed at shepherding immunity to produce broadly neutralizing antibodies to highly diversified pathogens such as HIV-1 and Influenza.

Introduction

Both the affinity and diversity of antibodies elicited by immunization or infection increase over time by a process that involves iterative cycles of selection, clonal expansion and somatic mutation in germinal centers (GCs) (Bannard and Cyster, 2017; Victora and Nussenzweig, 2022). These two apparently discordant features of humoral immune responses, increasing affinity and diversity, can be accounted for by dynamic changes in selection over time and by the existence of two cellular compartments, plasma cells and memory B cells respectively. Plasma cells develop by a mechanism that ensures increasing circulating antibody affinity (Zotos and Tarlinton, 2012; Nutt et al., 2015; Kräutler et al., 2017; Ise et al., 2018; Tas et al., 2022; ElTanbouly et al., 2024; MacLean et al., 2025). Memory B cells are selected by a separate mechanism that emphasizes diversity over affinity (Inoue et al., 2022, 2021; Suan et al., 2017; Viant et al., 2020; Wang et al., 2017).

Antibody diversification becomes increasingly important during secondary or booster immune responses, when only small numbers of high affinity antigen binding cells can be detected in GCs (Dal Porto et al., 2002; Eckl-Dorna et al., 2019; Mesin et al., 2019; Malladi et al., 2025). Given the strong selection pressure imposed by iterative cycles of mutation and cell division in the GC, the evolution away from high affinity is counterintuitive. However, diversification may be an important evolutionary adaptation to deal with rapidly changing pathogens such as Coronaviruses and Influenza virus (Heyman, 2000; Cyster and Wilson, 2024).

Several mechanisms have been suggested to account for the increase in diversity and loss of detectable antigen binding in late primary and secondary GCs. These include: 1. Continual recruitment of additional lower affinity cells during the reaction (De Carvalho et al., 2023; Hägglöf et al., 2023); 2. Increasing T cell fitness that lowers the threshold of B cell selection (Woodruff et al., 2018; Merkenschlager et al., 2023); 3. Antibody mediated antigen masking or enhancement (Heyman, 2000; Cyster and Wilson, 2024).

The effects of antibody feedback on immune responses have been studied since 1909 when they were first described by Theobald Smith in experiments on Diphtheria toxin (Smith, 1909). Recent data shows that masking appears to be mediated by high affinity antibodies and enhancement by low concentrations or low affinity antibodies that may be present even before immunization or in the early stages of the immune response (Heyman, 2000; Cyster and Wilson, 2024). But because all experiments to date, including Smith's, have been performed in organisms that have at least some level of circulating antibody, precisely how masking and enhancement contribute to the evolution of humoral immunity and GC dynamics remains to be determined. Understanding these phenomena is increasingly important in developing strategies for sequential vaccination for difficult pathogens such as malaria parasites, HIV-1 and influenza virus where antibody mediated masking can interfere with the evolution of immunity in response to serial vaccine boosters (Cyster and Wilson, 2024).

Here we examine the role of antibody feedback in regulating GC responses in mice that have an intact polyclonal B cell compartment but do not secrete antibodies.

90

91 ## Results

92 ### Antibody secretion-deficient mice

93 To examine how secreted antibodies impact the development of immune responses,
94 we engineered the IgH locus to produce two strains of mice: a control strain that
95 expresses membrane and secreted forms of IgM (M-only) but no other isotypes; and
96 a second strain whose B cells express only the membrane-bound form of IgM (mM-
97 only) (Fig. 1 A). To this end, the C57BL/6J Ig heavy chain locus was modified using
98 CRISPR-Cas9 to delete a 150 kb region 5' of *Ighd* exon 1 to the 3' UTR of *Igha*,
99 leaving only the IgM locus intact (M-only mice, see methods for further details). M-
100 only mice were subsequently engineered to produce the mM-only mice by removing
101 the stop codon of the secreted splice form and its intronic polyadenylation signal in
102 *Ighm* exon 4 (Danner and Leder, 1985; Nussenzweig et al., 1987; Boes et al., 1998;
103 Ehrenstein et al., 1998; Waisman et al., 2007). The later abrogates production of the
104 secreted form by preventing its termination thereby enforcing splicing to produce the
105 membrane-bound isoform of IgM. We focused on the IgM isotype because it does
106 not bind to most Fc receptors and therefore its Fc-mediated activity is generally more
107 limited than other isotypes.

108 Consistent with the observation that membrane-bound IgM regulates B cell
109 development in the bone marrow (Nussenzweig et al., 1987; Kitamura et al., 1991),
110 M-only and mM-only mice showed generally normal numbers of pro-B, pre-B,
111 immature and mature B cells in the bone marrow (Fig. 1 B and Fig. S1 A). Moreover,
112 the overall numbers of transitional and mature B2 cells in spleen were similar,
113 although a minor decrease of T2 cells was observed in mM-only mice. As reported

114 by others, mice lacking secreted Igs, show increases in splenic B1 and marginal zone
115 B cells but total numbers of B cells were similar in spleen, mesenteric lymph nodes
116 (mLN) and Peyer's patches. (Fig. 1 C-E and Fig. S1 B-G) (Hannum et al., 2000;
117 Anderson et al., 2006). κ/λ light chain ratios showed minor differences in mM-only
118 mice compared to both WT and M-only mice (Fig. S1 H). There were fewer plasma
119 cells in the bone marrow of M-only mice compared to WT and they were difficult to
120 detect in mM-only mice in (Fig. 1 F, Fig. S1 A). Serum ELISAs performed under steady
121 state conditions showed slightly increased IgM but no other isotypes in M-only mice
122 and no detectable antibody in mM-only mice (Fig. 1 G, P=0.0017). Despite the
123 absence of other isotypes, single-cell Ig mRNA sequencing did not reveal any notable
124 differences in Ighv, Igkv and Iglv usage by follicular B cells between wild type (WT),
125 M-only and mM-only mice except for an enrichment of Ighv7-3 in mM-only mice
126 compared to WT (Fig. 1 H and Fig. S1 I). mM-only B cells showed higher levels of
127 surface IgM expression in both bone marrow and the spleen possibly due to their lack
128 of IgD and inability to secrete (Fig. S1 J). Finally, at steady state, mLN GCs in mM-
129 and M-only mice had similar dark zone (DZ)/light zone (LZ) ratios and number of T
130 follicular helper (T_{FH}) cells (Fig. S1 K and L). In summary, B cell development appears
131 largely normal, but there are no serum antibodies and few if any plasma cells in mM-
132 only mice.
133
134 **Primary immune responses**
135 To determine how antibodies impact the development of primary B cell immune
136 responses we immunized mice with the Wuhan-Hu-1 SARS-Cov2 receptor binding
137 domain (RBD) (Fig. 2 A). Antigen-specific antibodies were measured by ELISA (Fig. 2

138 B-D). As expected, M-only mice were limited to the IgM isotype, and mM-only mice
139 produced no serum antibodies in response to the immunization (Fig. 2 B-D). The
140 kinetics of the serological response in M-only mice was similar to WT (Fig. 2 B and
141 D), but the total amount of antibody was lower when considering all isotypes (Fig. 2
142 B). Notably, whereas the total antibody levels in WT mice decreased over the 150-
143 day period of observation, serum Ig levels were relatively stable and even increased
144 modestly in M-only mice (Fig. 2 B).

145 Germinal center responses were analyzed by flow cytometry on days 0, 7, 14,
146 21 and 28 after immunization. GCs were absent from popliteal LNs before
147 immunization (Fig S2 A). The absolute numbers of B cells and the relative proportions
148 of germinal center B cells among B220^{+} B cells was similar among WT, M-only and
149 mM-only mice at all time point points analyzed (Fig. 2 E and F and Fig. S2 A-C). Thus,
150 the contribution of antibodies to GC magnitude and kinetics in the primary response
151 to SARS-CoV2-RBD appears to be limited.

152 Plasma cell precursors were evident in GCs of all 3 strains, but showed
153 increased caspase expression in mM-only mice and these mice had few detectable
154 mature plasma cells in lymph nodes (LNs) or bone marrow (Fig. 2 G-J and Fig. 1 F
155 and Fig. S2 D,E and Fig. S1 A). The data are consistent with the idea that plasma cells
156 that are unable to secrete antibody die by apoptosis (Iwakoshi et al., 2003; Todd et
157 al., 2009; Bonaud et al., 2023).

158 We analyzed the antigen-binding capacity of GC B cells in the primary
159 response by flow cytometry using the Wuhan-Hu-1 RBD labeled with 2 different
160 fluorophores (Fig. 2 K and L). At the peak of the GC response, 14 days after
161 immunization, there were similar proportions of RBD-binding cells in WT and M-only

162 mice (35 % and 26 % respectively), but significantly more in the GCs of mM-only
163 mice (45 % p=0.0021, Fig. 2 L and Fig. S2 F). Moreover, whereas antigen binding B
164 cells decreased over time in WT and M-only mice their relative proportion appeared
165 to persist in mM-only GCs (Fig. 2 L). Differences in BCR expression did not account
166 for this difference in antigen binding as IgM surface expression levels were equivalent
167 among genotypes (Fig. S2 G and H). The data is consistent with the idea that secreted
168 antibodies mask immunodominant epitopes and increase antigen valency, thus
169 curbing the relative competitive advantage of high-affinity immunodominant antigen
170 binding cells in the later stages of the primary GC reaction (Heyman, 2000; Andrews
171 et al., 2015; Schaefer-Babajew et al., 2023; Cyster and Wilson, 2024; Yan et al., 2025).
172 To gain further insights into the effect of antibodies on primary GC responses
173 we examined clonality, diversity and IgV gene usage by single cell VDJ sequencing
174 14 days after immunization. As expected, expanded clones of B cells were found in
175 GCs of all 3 genotypes (Fig. 3 A-C and G and Fig. S2 I). However, the individual clones
176 appeared to be larger and less diverse in the GCs of mM-only mice than in mice that
177 expressed secreted antibodies as evidenced by significant higher overall clonality
178 and a decrease in the fraction of individual sequences (Fig. 3 B-C). Consistent with
179 this observation mM-only GC B cells showed reduced Shannon and Inverse Simpson
180 diversity indices, but similar levels of somatic mutation compared to their
181 counterparts, even when analyzing the sequences of clones composed from the top
182 10 most frequent V genes in mM-only mice (Fig. 3 D-F and Fig. S2 J). We did not
183 detect significant skewing of IgV gene usage (Fig. 3 G and Fig. S2 K). In conclusion,
184 secreted antibodies appear to be essential for B cell repertoire diversification in

185 primary GC responses to SARS-CoV2 RBD – a mechanism that appears to be
186 significant even at the early stages of the response.
187
188 **Secondary Immune Responses**
189 To determine whether antibodies developing during the primary response influence
190 subsequent booster responses, we vaccinated WT, M-only and mM-only mice in
191 accordance with protocols used during human immunization against SARS-CoV-2
192 using full-length stabilized SARS-CoV-2 spike protein (Fig. 4 A).
193 Serum antibody responses were measured by ELISA at approximately weekly
194 intervals from days 6 to 97 after immunization. As in the primary responses,
195 antibodies were not detectable in mM-only mice (Fig. 4 B and Fig. S3 A), and M-only
196 mice produced approximately 30-fold less serum antibody compared to WT mice 14
197 days after boosting. Flow cytometry on cells obtained from draining lymph nodes
198 showed that M-only had lower proportions of GC B cells, but mM-only was not
199 significantly different from WT (Fig. 4 C). Thus, the complete absence of secreted
200 antibodies does not impact the ability to form or sustain secondary GCs.
201 Antigen-binding GC B cells were enumerated using fluorescently labeled
202 Wuhan-Hu-1 RBD since this is the primary target of the anti-Spike immune response
203 in mice and humans. Notably, the 3 strains differed significantly in the fraction of
204 Wuhan-Hu-1 RBD-binding B cells (Fig.4 D). Whereas only 1.9 % and 3 % of the B
205 cells in WT or M-only GCs bound to RBD, 22 % of mM-only GC B cells showed
206 demonstrable binding ($p= 0.002$, Fig. 4 D).
207 To determine the antigen-binding specificity of GC B cells that develop after
208 boosting, we cloned and expressed 146 representative antibodies and tested them

209 for binding to Wuhan-Hu-1 spike and the isolated RBD by ELISA (Table S1).
210 Altogether, only 17 % (wild-type) and 25 % (M-only) of mAbs isolated from secondary
211 GCs exposed to endogenous antibodies showed measurable binding to the
212 immunizing antigen, whereas 54 % of the mAbs isolated from mM-only GCs were of
213 sufficiently high affinity to bind by ELISA (Fig. 4 E and Fig. S3 B). Whereas 32 % of
214 antibodies obtained from mM-only mice bound to the immunodominant RBD, only
215 4.2 % and 2.1 % of mAbs from WT and M-only GCs did so, respectively (p=0.0002
216 and 0.0005 respectively, Fig. 4 E). The fraction of antibodies binding to non-RBD
217 epitopes on the spike was 12.5 %, 23 % and 22 % in WT, M-only and mM-only mice,
218 respectively. To examine the nature of the antibodies produced after booster
219 immunization, we compared the Ig sequences from single GC B cells. GC B cells
220 obtained from secondary GCs of mM-only mice were more clonal and significantly
221 less diverse than those obtained from M-only mice (Fig. 4 F-I). Again, we did not
222 detect significant differences in V gene usage and genotypes displayed similar
223 numbers of somatic mutations (Fig 4 J and Fig. S3 C). The data suggest that antibody
224 feedback inhibits accumulation of GC B cells that are restricted to the initial
225 immunodominant epitope even when those antibodies are restricted to the IgM
226 isotype and when total Ig concentrations are 30-fold lower than physiologic.

227 To determine whether passively transferred antibodies are sufficient to revert
228 the mM-only phenotype, we repeated the prime boost experiment with Wuhan-Hu-1
229 spike and transferred contemporaneous serum from WT mice into mM-only
230 recipients (Fig. 4 K). As determined by ELISA serologic reconstitution was only partial
231 with an approximately 10-fold lower level of specific antibodies in the mM-only
232 recipients compared to their WT counterparts (Fig. S4 A). Notably, while the fraction

233 of GC B cells in draining LNs was similar between genotypes, passive antibody
234 transfer completely reverted the mM-only phenotype resulting in near complete loss
235 of Wuhan-Hu-1 RBD binding B cells in the mM-only GCs (Fig. 4 L and M and Fig. S4
236 B and C). We conclude that small amounts of polyclonal antigen-specific serum is
237 sufficient to drastically change antigen binding specificity in the GC. This observation
238 is consistent with the idea that secreted antibodies mask immunodominant epitopes
239 and thereby diversify epitope usage in GCs during polyclonal immune responses.

240 Sequential immunization strategies designed to produce broadly neutralizing
241 antibodies (bNAbs) to HIV-1 and influenza virus are currently being investigated in
242 animal models and in the clinic. The multi-step vaccine concept being tested involves
243 using mutated, high-affinity priming immunogens to recruit rare bNAb precursors
244 followed by iterative administration of progressively more native antigens to shepherd
245 B cell responses through a series of somatic mutations required to produce bNAbs
246 (Escolano et al., 2016; Burton, 2019; Haynes et al., 2023). At the end of the sequence,
247 antigen binding B cells should retain binding to the priming immunogen and in
248 addition bind to all the different antigens used in the vaccine. This idea has yet to
249 produce necessary broadly protective serologic responses in part because "off
250 target" antibodies to alternative sites on the immunogen dominate the response after
251 booster vaccination (Escolano et al., 2019, 2021). To determine how circulating
252 antibodies might contribute to this effect, we immunized mice with a series of 4 HIV-
253 1 CD4-binding site-targeting immunogens, the first of which is currently in early
254 clinical testing (NCT05471076; 426c.DMRS.Core (TM4) antigen, Fig. 5 A) (McGuire et
255 al., 2016). Immunizations were administered in the same anatomic location
256 throughout and longitudinal ELISA analysis for antibodies binding to

257 426c.DMRS.Core showed that titers were present throughout the immunization
258 protocol in WT and M-only but not mM-only mice (Fig. 5 B).
259 14 days after the last boost GC B cell numbers were equivalent among the 3
260 mouse strains with median GC B cell frequencies between 1.7 % to 2.2 % of all B
261 cells in the draining lymph node (Fig. 5 C and Fig. S5 A). Somatic hypermutation was
262 again comparable across genotypes including expanded clones (Fig. 5 D and Fig. S5
263 B). Clonality, clone size, IgV gene usage and measures of diversity did not show
264 significant differences (Fig. 5 E-I and Fig. S5 C), and considering all cells irrespective
265 of HIV-1 antigen-binding, we saw a high degree of clonality in all 3 groups (Fig. 5 E).
266 Antigen binding to TM4, but not to other sequentially delivered antigens was
267 measured by flow cytometry. Notably, at the end of the sequential vaccine sequence
268 WT, M-only and mM-only showed 0.76 %, 3 % and 9 % TM4-binding GC cells
269 respectively (Fig. 5 J and Fig. S5 D). Thus, only mM-only mice that are devoid of
270 circulating antibodies show continued levels of GC B cells that bind to the priming
271 immunogen after a sequential series of HIV-1 vaccine boosters. In summary antibody
272 feedback interfered strongly with persistence of antigen binding GC B cells in
273 sequential immunization but differences in clonality and diversity were less
274 pronounced compared to repeated SARS-CoV-2 spike protein immunization. We
275 speculate that this difference arises partly from the nature of the antigens and
276 reduced antibody feedback associated with the sequential use of different antigens.
277 We conclude that circulating antibodies interfere with GC persistence of B cells that
278 retain the ability to bind to the priming immunogen.
279
280

281 ## Discussion

282 GCs are microanatomic compartments specialized for affinity maturation and
283 diversification of humoral immune responses. Affinity maturation is an iterative
284 process involving repetitive cycles of division and mutation in the GC dark zone
285 followed by migration to the light zone where B cells test their newly acquired antigen
286 receptors for binding and capture of antigen deposited in follicular dendritic cells.
287 Selection is mediated by a combination of B cell receptor signaling and T follicular
288 help (Victora and Nussenzweig, 2022; Chen et al., 2023). How GCs diversify antibody
289 responses in the face of strong positive selection is less well understood. Our data
290 indicate that even small amounts of specific polyclonal antibodies produced during
291 the immune response are sufficient to diversify the GC. We hypothesize that this
292 phenomenon is due to masking responses to immunodominant epitopes and by
293 producing immune complexes that lower the affinity thresholds for B cell entry into
294 the GC.

295 Antibody feedback has been studied primarily by passive antibody transfer in animals
296 and humans (Heyman, 2000; Schaefer-Babajew et al., 2023; Cyster and Wilson,
297 2024). These experiments revealed that both IgM and IgG can produce immune
298 complexes and mediate masking through interactions with Fc and complement
299 receptors (Heyman, 2000). Moreover, recent work in antibody knock in mice
300 producing antibodies of differing affinity to a selected epitope showed that the
301 antibody feedback effects were dependent on affinity and that changes in the T cell
302 compartment might also contribute (Barbulescu et al., 2025; Yan et al., 2025). In
303 addition, even partial deletion of antibody secreting cells showed that masking
304 impacts the composition of the GC (Schiepers et al., 2024). Our experiments extend

305 these findings to primary and secondary immune responses in animals that have an
306 otherwise intact polyclonal B and T cell compartment but are unable to produce
307 secreted antibodies. Our data show that antibody feedback is a major mechanism for
308 diversification of both primary and secondary humoral immune responses.
309
310 Diversification by antibody feedback has the potential to enable recall responses to
311 rapidly evolving pathogens. For example, although initial responses to SARS-CoV-2
312 were focused on highly strain specific epitopes, antibody feedback diversified the
313 response to include more conserved epitopes that offered some protection against
314 newly arising variants. However, our data indicate that these feedback effects pose
315 a very significant barrier to sequential immunization approaches such as those being
316 tested for HIV-1 that aim to focus immunity to a singular broadly neutralizing epitope.
317

318 ## Methods

319 ### Mice

320 C57BL/6J mice were purchased from Jackson Laboratories. M-only and mM-only
321 mice were created and maintained at the Rockefeller University with assistance from
322 the Rockefeller University CRISPR and Genome Editing Center and Transgenic and
323 Reproductive Technology Center. Cas9 (IDT) and sgRNA (IDT) ribonucleoprotein
324 complexes targeting the IgH locus were electroporated into C57BL6/J single cell
325 mouse embryos, which were then recovered and incubated overnight at 37°C before
326 implantation into female foster mother mice. For M-only mice sgRNA spacer
327 sequences GTAGATCTCTTCCTAAGAGG and TTACTAGGCTCCTCCATATG were
328 used to delete *Ighd–Igha*. M-only mice were retargeted and with sgRNAs with spacer

329 sequences CGCCTGTGTCAGACATGATC and GGGTAGGACAAGCAACGCAC to
330 delete the part of *Ighm* exon 4 only found in the secreted IgM splice form, as well as
331 the subsequent stop codon and alternative, intronic polyadenylation site (Danner and
332 Leder, 1985; Boes *et al.*, 1998; Ehrenstein *et al.*, 1998; Waisman *et al.*, 2007). Cutsite
333 adjacent deletions were verified by PCR from tail DNA and Sanger sequencing of
334 PCR products. Sequences were analyzed using Geneious Prime (GraphPad). Mice
335 were bred to homozygosity. Presence or absence of antibody isotypes was verified
336 by flow cytometry and ELISA of serum in homozygous animals from homozygous
337 parents due to maternal transfer of antibodies in utero and through suckling.
338 Male and female mice aged 6-12 weeks were used. Animals were housed at the
339 Rockefeller University Comparative Bioscience Center and all animal procedures
340 were performed following protocols approved by the Rockefeller University
341 Institutional Animal Care and Use Committee. Animals were housed at an ambient
342 temperature of 22 °C and a humidity of 30–70 % under a 12 h–12 h light–dark cycle
343 with free access to food and water. For experimental endpoints, mice were
344 euthanized using CO_2, followed by cervical dislocation.
345
346 **Immunization**
347 All immunizations were performed by subcutaneous footpad injection of 5 µg of
348 immunogen in 33 % alhydrogel (Invivogen).
349
350 **Serum infusion**

351 Serum was obtained from immunized, time-matched C57BL/6J mice and pooled,
352 before being administered to recipients at the equivalent time points. Each recipient
353 received 200 μL of the pooled serum on a weekly basis.
354
355 **Flow cytometry**
356 For steady state experiments, mice aged from 10 to 11 weeks were sacrificed and
357 their spleen, mesenteric LN, Peyer's patches and bone marrow were isolated and
358 dissociated to obtain single-cell suspensions. Bone marrow from pelvic bone, femur
359 and tibia was isolated by centrifugation at 10,000 g for 15 s. Spleen and Peyer's
360 patches were forced through a 70 μm cell strainer. LNs were collected into 1.5 mL
361 Eppendorf tubes and dissociated using a pestle. Spleen and bone marrow pellets
362 were then incubated in ACK lysis buffer for 15 min on ice, washed and processed
363 together with the LN as described below.
364 For all experiments, single cell suspensions were incubated in Fc block (BD
365 Biosciences) for 15 min. Cells were then centrifuged at 350 g for 5 min and
366 resuspended and incubated in a solution of PBS diluted fluorescent-Biotin-antigen
367 tetramers for 30 min on ice. Additional labeled antibodies were then added to the
368 cells and samples were incubate for 30 additional minutes on ice. For intracellular
369 staining of Caspase 3, cells were permeabilized using eBioscience Foxp3
370 permeabilization kit (reference: 00-5523-00), washed in the supplied permeabilization
371 buffer and stained for 30 min at 4 °C. as per manufacturer's instructions. The different
372 cell populations were identified as follows: ProB (Dump$^-$, CD19$^+$, B220$^+$, IgM$^-$, CD2$^-$),
373 PreB (Dump$^-$, CD19$^+$, B220$^+$, IgM$^-$, CD2$^+$), Immature B (Dump$^-$, CD19$^+$, B220$^+$, IgM$^+$,
374 CD2$^+$, CD23$^-$), Mature B (Dump$^-$, CD19$^+$, B220$^+$, IgM$^+$, CD2$^+$, CD23$^+$), B1a (Dump$^-$,

375 CD19^{+}, B220^{-}, CD23^{-}, CD5^{+}), B1b (Dump^{-}, CD19^{+}, B220^{-}, CD23^{-}, CD5^{-}), B2 (Dump^{-},
376 CD19^{+}, B220^{+}), Transitional B (Dump^{-}, CD19^{+}, B220^{+}, CD93^{+}), pre-marginal zone B
377 (Dump^{-}, CD19^{+}, B220^{+}, CD21^{hi}, CD93^{-}, IgM^{hi}, CD23^{+}), marginal zone B (Dump^{-}, CD19^{+},
378 B220^{+}, CD21^{hi}, CD93^{-}, IgM^{hi}, CD23^{-}), Follicular B (Dump^{-}, CD19^{+}, B220^{+}, CD21^{int},
379 CD93^{-}, IgM^{+}), PC at steady state (Dump^{-}, CD98^{+}, TACI^{+}) or after immunization (Dump^{-}
380 CD98^{+} CD138^{+}), GC B cells (Dump^{-}, CD98^{-}, CD138^{-}, B220^{+}, CD95^{+}, CD38^{-}). The Dump
381 channel contains Ly6G, F4/80, NK1.1, CD4, CD8 antibodies and Zombie-NIR
382 live/dead marker. Flow cytometric reagents are listed in Table S2.
383 Antigen tetramer staining was performed with a combination of two different
384 fluorescently-labelled streptavidin conjugates per antigen. Biotinylated antigens at
385 5 µg/mL were individually pre-incubated with each streptavidin-fluorophore (all
386 Biolegend) at a 1 µg/mL dilution before staining to allow tetramer formation, then
387 combined and cells resuspend in the mixture and incubated for 30 min on ice, before
388 staining for other surface markers. Samples were acquired on a BD LSRFortessa or
389 BD Symphony A3 or A5. All cell sorting was performed on the BD FACSymphony S6.
390 Data was analyzed using FlowJo 10.10.0.
391
392 **Recombinant protein production**
393 All expression vectors for recombinant protein production were confirmed by Sanger
394 (Azenta) or Oxford Nanopore sequencing (Plasmidsaurus). The construct encoding
395 the RBD of SARS-CoV-2 (GenBank MN985325.1; S protein residues 319–539) was
396 previously described (Barnes et al., 2020). All recombinant proteins were produced in
397 Expi293F cells (Gibco, A14527), except 426c.WT.SOSIP which was produced in
398 Expi293F GnTI- cells (Gibco, A39240). Transient transfections of expression plasmids

399 were performed using Expifectamine 293 transfection kit (Gibco, A14525) as
400 previously described (McGuire et al., 2014). In brief, 4-6 days post transfection,
401 culture supernatant was harvested, centrifuged to pellet cells and sterilized by
402 filtration for affinity chromatography. Trimeric Env proteins were purified by passing
403 the supernatant through an agarose-bound *Galanthus nivalis* lectin (GNL) resin
404 (Vector Laboratories) and subsequent size-exclusion chromatography (SEC). A Ni
405 Sepharose 6 Fast Flow resin (Cytiva, 117531803) was used for purification of His-
406 tagged proteins. Native gel electrophoresis identified peak fractions from size-
407 exclusion chromatography. Fractions corresponding to monomeric Envelope trimers,
408 Spike S6P protein trimers or RBD monomers were pooled and stored at -20 °C.
409 Antibodies were purified over a protein G Sepharose 4Fast Flow resin (Cytiva
410 70611805) and buffer exchanged into PBS and stored at -80 °C.
411 For random biotinylation, proteins were biotinylated using the EZ-Link-Sulfo-NHS-
412 LC-Biotinylation kit according to the manufacturer's instructions (Thermo Fisher
413 Scientific, 31497). Excess biotin was removed by diafiltration with 100 kDa cutoff.
414 Biotinylated protein was stored at -20 °C or -80 °C.
415 Avi-tagged TM4 core gp120 or RBD were biotinylated using a BirA reaction according
416 to the manufacturer's instructions using a 5-fold molar excess of biotin (Avidity,
417 EC6.3.4.15), buffer exchanged to PBS and stored at -80°C.
418
419 **ELISA**
420 All ELISAs used Costar 96-well, half area, high binding, polystyrene assay plates
421 (Corning, Cat.# 3960), which were coated with the indicated antigen (TM4, SARS-
422 CoV-2 Wuhan-Hu-1 RBD or spike protein, all produced in house) or anti-isotype

423 antibody (anti-IgM, Southern Biotech, 1020-01; anti-IgG3, Southern Biotech, 1100-
424 01; anti-IgG1, Southern Biotech, 1070-01; anti-IgG2b, Southern Biotech, 1090-01;
425 anti-IgG2c, Jackson Immunoresearch, 115-005-208; anti-IgA, Southern Biotech,
426 1040-01) at 2 – 5 µg/mL in PBS over night at 4°C. Plates were blocked with 5 %
427 skimmed milk powder in PBS or 1 % BSA 0.1 mM EDTA 0.05 % Tween20 in PBS for
428 2 h at room temperature. 6 washes in PBS 0.05 % Tween 20 were performed after
429 every subsequent step. Sera were diluted in PBS at 1:50 to 1:100 top dilution and 1:3
430 (naïve and after prime) or 1:4 (after boosts) or 1:5 (steady state serum antibody levels)
431 serially diluted for an 8-point curve. Isotype antibody standards (Southern Biotech
432 5300-01B) were diluted to 10 µg/mL and diluted 1:5 in PBS for an 8-point curve.
433 Secondary antibodies conjugated to horseradish peroxidase were used to detect
434 bound antibodies mouse IgG (1:5000, Jackson ImmunoResearch Cat.# 115-035-071
435 or Southern Biotech Cat.# 1030-05) or mouse IgM, IgG3, IgG1, IgG2b, or IgA
436 (Southern Biotech Cat.# 5300-05B) or IgG2c (Jackson ImmunoResearch 115-035-
437 208) or total Ig (anti-kappa combined with anti-lambda light chain, Southern Biotech
438 Cat.# 5300-05B). HRP substrate 3,3',5,5'-tetramethylbenzidine substrate
439 (ThermoFisher, Cat.# 34021) was used for development and the reaction was
440 stopped adding an equal volume of 1 M H_2SO_4 (Sigma). Absorbance was read at
441 450 nm and 570 nm on a FLUOstar Omega (BMG Labtech). For analysis of steady
442 state antibody concentration in serum, isotype standards were included on every
443 plate and used to fit a sigmoidal 4-parameter logistic regression standard curve in
444 GraphPad Prism 10 which was used to interpolate serum concentrations from
445 dilutions in the exponential phase of the curve. For total anti-antigen responses,
446 sigmoidal 4-parameter logistic regression was fitted to curves of every sample and

447 used to calculate the half maximal binding titer (BT_{50}). µg/mL values below detection
448 were set to minimum detection level based on control sera to avoid plotting 0 on
449 logarithmic plots. For samples where signal was too low for a curve fit BT_{50} was set
450 to 10, which is 5x above the highest measured dilution.
451

452 **10x genomics and single-cell libraries**

453 Indicated mice were immunized with either Spike, RBD or HIV proteins. Cell
454 suspensions were prepared as mentioned before from popliteal lymph nodes and
455 samples were indexed using TotalSeqC cell surface antibodies (Biolegend). Live,
456 $Dump^-$ B cells ($CD38^+$, GC B cells RBD^+ and GCB RBD^-), and PC were then isolated
457 flow cytometry and loaded onto the Chromium Controller from 10x Genomics.
458 scRNA-seq libraries were prepared using the Chromium Single Cell 5′ v.2 Reagent
459 Kit (10x Genomics) according to the manufacturer's protocol. Libraries were loaded
460 onto an Illumina NovaSeq for single-cell gene expression (GEX), VDJ analysis and
461 hashtags (HTO) library at the Rockefeller University Genomics Resource Center.
462 Hashtag indexing from TotalSeqC antibodies was used to demultiplex the
463 sequencing data and generate gene and barcode matrices, respectively.
464 All single-cell BCR libraries were mapped to the Cell Ranger VDJ GRCm38 reference
465 using Cell Ranger multi v.8.1.0 (10x genomics). Contigs containing less than 50 reads
466 and more than one heavy or light chain were removed. Antibodies heavy and light
467 chains were paired using in-house scripts, and further analyzed using igpipeline v.3
468 (https://github.com/stratust/igpipeline/tree/igpipeline3) to define clonotypes, as
469 previously described (Wang et al., 2023), using the mouse IMGT database as
470 reference (Lefranc, 2011).

471 For the primary response dataset analyses (Fig. 1 H and Fig. 3), scRNA-seq and
472 Hashtag-oligos unique molecular identifier quantification were performed with Cell
473 Ranger multi v.8.0.1 using the Cell Ranger GEX reference mm10, and analyzed in R
474 with Seurat v.5.1.0 (Hao et al., 2021). Cells were demultiplexed with
475 MULTISeqDemux, and those classified as doublets or with mitochondrial content
476 greater than 10 % and feature count less than 1,000 or greater than 6,500 were
477 excluded. Cell cycle genes were regressed out. Sample batches were then merged,
478 scaled and normalized with SCTransform. B cell (*Cd19, Ms4a1, Cd79a, Tnfrsf13c,*
479 *Aicda, Lyz2, Cd63*), Follicular (*Cd38, Cd55, Bcl2, Maml2, Notch2, Gpr183, Sell, Ccr6*),
480 and memory B cell (Binet et al., 2024) signatures were assigned using
481 AddModuleScore. Cells with low B cell module score (≤ 25th percentile) or with high
482 memory B cell score (≥ 75th percentile) were excluded. B cells expressing *Bcl6,*
483 *Aicda, S1pr2* or *Fas* at high levels (≥ 75th percentile) were classified as GC B cells,
484 whereas those with high follicular score (≥ 75th percentile) were classified as follicular
485 B cells.
486
487 **Statistical analysis**
488 Details of statistics including tests used, exact values and n numbers are indicated in
489 figure legends and/or main text. Quantification and statistical analyses were
490 performed in R (v4.4.0) with Rstudio server (2024.04.0 Build 735) and/or GraphPad
491 Prism (Version 10.2.3), unless otherwise detailed in this methods section. Graphs
492 generated using Prism and R were assembled into figures using Adobe Illustrator.
493 Flow cytometry analysis was performed in FlowJo v.10.10.0 software (BD).
494

References

Anderson, S.M., L.G. Hannum, and M.J. Shlomchik. 2006. Cutting Edge: Memory B Cell Survival and Function in the Absence of Secreted Antibody and Immune Complexes on Follicular Dendritic Cells. *The Journal of Immunology*. 176:4515–4519. doi:10.4049/jimmunol.176.8.4515.

Andrews, S.F., K. Kaur, N.T. Pauli, M. Huang, Y. Huang, and P.C. Wilson. 2015. High Preexisting Serological Antibody Levels Correlate with Diversification of the Influenza Vaccine Response. *J Virol*. 89:3308–3317. doi:10.1128/JVI.02871-14.

Bannard, O., and J.G. Cyster. 2017. Germinal centers: programmed for affinity maturation and antibody diversification. *Current Opinion in Immunology*. 45:21–30. doi:10.1016/j.coi.2016.12.004.

Barbulescu, A., J. Bilanovic, T. Langelaar, A.K. Teetz, L. Urnavicius, A. Hobbs, J.-J. Shen, N.H. Abrahamse, R.V.H. De Carvalho, L. Mesin, C.L. Ferreira, J. Bortolatto, and G.D. Victora. 2025. Antibody-mediated feedback modulates interclonal competition in the germinal center. doi:10.1101/2025.11.06.686519.

Barnes, C.O., A.P. West, K.E. Huey-Tubman, M.A.G. Hoffmann, N.G. Sharaf, P.R. Hoffman, N. Koranda, H.B. Gristick, C. Gaebler, F. Muecksch, J.C.C. Lorenzi, S. Finkin, T. Hägglöf, A. Hurley, K.G. Millard, Y. Weisblum, F. Schmidt, T. Hatziioannou, P.D. Bieniasz, M. Caskey, D.F. Robbiani, M.C. Nussenzweig, and P.J. Bjorkman. 2020. Structures of Human Antibodies Bound to SARS-CoV-2 Spike Reveal Common Epitopes and Recurrent Features of Antibodies. *Cell*. 182:828-842.e16. doi:10.1016/j.cell.2020.06.025.

Binet, L., C. Dong, N. Attaf, L. Gil, M. Fallet, T. Boudier, B. Escalière, L. Chasson, C. Siret, S. Van De Pavert, J.-M. Navarro, and P. Milpied. 2024. Specific pre-plasma cell states and local proliferation at the dark zone - medulla interface characterize germinal center-derived plasma cell differentiation in lymph node. doi:10.1101/2024.07.26.605240.

Boes, M., C. Esau, M.B. Fischer, T. Schmidt, M. Carroll, and J. Chen. 1998. Enhanced B-1 cell development, but impaired IgG antibody responses in mice deficient in secreted IgM. *J Immunol*. 160:4776–4787.

Bonaud, A., L. Gargowitsch, S.M. Gilbert, E. Rajan, P. Canales-Herrerias, D. Stockholm, N.F. Rahman, M.O. Collins, H. Taskiran, D.L. Hill, A. Alloatti, N. Alouche, S. Balor, V. Soldan, D. Gillet, J. Barbier, F. Bachelerie, K.G.C. Smith, J. Jellusova, P. Bruhns, S. Amigorena, K. Balabanian, M.A. Linterman, A.A. Peden, and M. Espéli. 2023. Sec22b is a critical and nonredundant regulator of plasma cell maintenance. *Proc. Natl. Acad. Sci. U.S.A.* 120:e2213056120. doi:10.1073/pnas.2213056120.

534 Burton, D.R. 2019. Advancing an HIV vaccine; advancing vaccinology. *Nat Rev*
535 *Immunol*. 19:77–78. doi:10.1038/s41577-018-0103-6.

536 Chen, S.T., T.Y. Oliveira, A. Gazumyan, M. Cipolla, and M.C. Nussenzweig. 2023. B
537 cell receptor signaling in germinal centers prolongs survival and primes B cells
538 for selection. *Immunity*. 56:547-561.e7. doi:10.1016/j.immuni.2023.02.003.

539 Cyster, J.G., and P.C. Wilson. 2024. Antibody modulation of B cell responses—
540 Incorporating positive and negative feedback. *Immunity*. 57:1466–1481.
541 doi:10.1016/j.immuni.2024.06.009.

542 Dal Porto, J.M., A.M. Haberman, G. Kelsoe, and M.J. Shlomchik. 2002. Very Low
543 Affinity B Cells Form Germinal Centers, Become Memory B Cells, and
544 Participate in Secondary Immune Responses When Higher Affinity
545 Competition Is Reduced. *Journal of Experimental Medicine*. 195:1215–1221.
546 doi:10.1084/jem.20011550.

547 Danner, D., and P. Leder. 1985. Role of an RNA cleavage/poly(A) addition site in the
548 production ofmembrane-bound and secreted IgM mRNA. *Proceedings of the*
549 *National Academy of Sciences*. 8658–8662.

550 De Carvalho, R.V.H., J. Ersching, A. Barbulescu, A. Hobbs, T.B.R. Castro, L. Mesin,
551 J.T. Jacobsen, B.K. Phillips, H.-H. Hoffmann, R. Parsa, M.C.C. Canesso, C.R.
552 Nowosad, A. Feng, S.R. Leist, R.S. Baric, E. Yang, P.J. Utz, and G.D. Victora.
553 2023. Clonal replacement sustains long-lived germinal centers primed by
554 respiratory viruses. *Cell*. 186:131-146.e13. doi:10.1016/j.cell.2022.11.031.

555 Eckl-Dorna, J., S. Villazala-Merino, B. Linhart, A.V. Karaulov, Y. Zhernov, M. Khaitov,
556 V. Niederberger-Leppin, and R. Valenta. 2019. Allergen-Specific Antibodies
557 Regulate Secondary Allergen-Specific Immune Responses. *Front. Immunol.*
558 9:3131. doi:10.3389/fimmu.2018.03131.

559 Ehrenstein, M.R., T.L. O'Keefe, S.L. Davies, and M.S. Neuberger. 1998. Targeted
560 gene disruption reveals a role for natural secretory IgM in the maturation of the
561 primary immune response. *Proc Natl Acad Sci U S A*. 95:10089–10093.
562 doi:10.1073/pnas.95.17.10089.

563 ElTanbouly, M.A., V. Ramos, A.J. MacLean, S.T. Chen, M. Loewe, S. Steinbach, T.
564 Ben Tanfous, B. Johnson, M. Cipolla, A. Gazumyan, T.Y. Oliveira, and M.C.
565 Nussenzweig. 2024. *Journal of Experimental Medicine*. 221:e20231838.
566 doi:10.1084/jem.20231838.

567 Escolano, A., H.B. Gristick, M.E. Abernathy, J. Merkenschlager, R. Gautam, T.Y.
568 Oliveira, J. Pai, A.P. West, C.O. Barnes, A.A. Cohen, H. Wang, J. Golijanin, D.
569 Yost, J.R. Keeffe, Z. Wang, P. Zhao, K.-H. Yao, J. Bauer, L. Nogueira, H. Gao,
570 A.V. Voll, D.C. Montefiori, M.S. Seaman, A. Gazumyan, M. Silva, A.T. McGuire,
571 L. Stamatatos, D.J. Irvine, L. Wells, M.A. Martin, P.J. Bjorkman, and M.C.
572 Nussenzweig. 2019. Immunization expands B cells specific to HIV-1 V3 glycan
573 in mice and macaques. *Nature*. 570:468–473. doi:10.1038/s41586-019-1250-
574 z.

575 Escolano, A., H.B. Gristick, R. Gautam, A.T. DeLaitsch, M.E. Abernathy, Z. Yang, H.
576 Wang, M.A.G. Hoffmann, Y. Nishimura, Z. Wang, N. Koranda, L.M. Kakutani,
577 H. Gao, P.N.P. Gnanapragasam, H. Raina, A. Gazumyan, M. Cipolla, T.Y.
578 Oliveira, V. Ramos, D.J. Irvine, M. Silva, A.P. West, J.R. Keeffe, C.O. Barnes,
579 M.S. Seaman, M.C. Nussenzweig, M.A. Martin, and P.J. Bjorkman. 2021.
580 Sequential immunization of macaques elicits heterologous neutralizing
581 antibodies targeting the V3-glycan patch of HIV-1 Env. *Sci. Transl. Med.*
582 13:eabk1533. doi:10.1126/scitranslmed.abk1533.

583 Escolano, A., J.M. Steichen, P. Dosenovic, D.W. Kulp, J. Golijanin, D. Sok, N.T.
584 Freund, A.D. Gitlin, T. Oliveira, T. Araki, S. Lowe, S.T. Chen, J. Heinemann, K.-
585 H. Yao, E. Georgeson, K.L. Saye-Francisco, A. Gazumyan, Y. Adachi, M.
586 Kubitz, D.R. Burton, W.R. Schief, and M.C. Nussenzweig. 2016. Sequential
587 Immunization Elicits Broadly Neutralizing Anti-HIV-1 Antibodies in Ig Knockin
588 Mice. *Cell*. 166:1445-1458.e12. doi:10.1016/j.cell.2016.07.030.

589 Hägglöf, T., M. Cipolla, M. Loewe, S.T. Chen, E.E. Kara, L. Mesin, H. Hartweger, M.A.
590 ElTanbouly, A. Cho, A. Gazumyan, V. Ramos, L. Stamatatos, T.Y. Oliveira,
591 M.C. Nussenzweig, and C. Viant. 2023. Continuous germinal center invasion
592 contributes to the diversity of the immune response. *Cell*. 186:147-161.e15.
593 doi:10.1016/j.cell.2022.11.032.

594 Hannum, L.G., A.M. Haberman, S.M. Anderson, and M.J. Shlomchik. 2000. Germinal
595 Center Initiation, Variable Gene Region Hypermutation, and Mutant B Cell
596 Selection without Detectable Immune Complexes on Follicular Dendritic Cells.
597 *The Journal of Experimental Medicine*. 192:931–942.
598 doi:10.1084/jem.192.7.931.

599 Hao, Y., S. Hao, E. Andersen-Nissen, W.M. Mauck, S. Zheng, A. Butler, M.J. Lee, A.J.
600 Wilk, C. Darby, M. Zager, P. Hoffman, M. Stoeckius, E. Papalexi, E.P. Mimitou,
601 J. Jain, A. Srivastava, T. Stuart, L.M. Fleming, B. Yeung, A.J. Rogers, J.M.
602 McElrath, C.A. Blish, R. Gottardo, P. Smibert, and R. Satija. 2021. Integrated
603 analysis of multimodal single-cell data. *Cell*. 184:3573-3587.e29.
604 doi:10.1016/j.cell.2021.04.048.

605 Haynes, B.F., K. Wiehe, P. Borrow, K.O. Saunders, B. Korber, K. Wagh, A.J.
606 McMichael, G. Kelsoe, B.H. Hahn, F. Alt, and G.M. Shaw. 2023. Strategies for
607 HIV-1 vaccines that induce broadly neutralizing antibodies. *Nat Rev Immunol*.
608 23:142–158. doi:10.1038/s41577-022-00753-w.

609 Heyman, B. 2000. Regulation of Antibody Responses via Antibodies, Complement,
610 and Fc Receptors. *Annu. Rev. Immunol.* 18:709–737.
611 doi:10.1146/annurev.immunol.18.1.709.

612 Inoue, T., R. Shinnakasu, C. Kawai, W. Ise, E. Kawakami, N. Sax, T. Oki, T. Kitamura,
613 K. Yamashita, H. Fukuyama, and T. Kurosaki. 2021. Exit from germinal center
614 to become quiescent memory B cells depends on metabolic reprograming and
615 provision of a survival signal. *Journal of Experimental Medicine*.
616 218:e20200866. doi:10.1084/jem.20200866.

617 Inoue, T., R. Shinnakasu, and T. Kurosaki. 2022. Generation of High Quality Memory
618 B Cells. *Front. Immunol.* 12:825813. doi:10.3389/fimmu.2021.825813.

619 Ise, W., K. Fujii, K. Shiroguchi, A. Ito, K. Kometani, K. Takeda, E. Kawakami, K.
620 Yamashita, K. Suzuki, T. Okada, and T. Kurosaki. 2018. T Follicular Helper Cell-
621 Germinal Center B Cell Interaction Strength Regulates Entry into Plasma Cell
622 or Recycling Germinal Center Cell Fate. *Immunity*. 48:702-715.e4.
623 doi:10.1016/j.immuni.2018.03.027.

624 Iwakoshi, N.N., A. Lee, and L.H. Glimcher. 2003. The X-box binding protein-1
625 transcription factor is required for plasma cell differentiation and the unfolded
626 protein response. *Immunological Reviews*. 194:29–38. doi:10.1034/j.1600-
627 065X.2003.00057.x.

628 Kitamura, D., J. Roes, R. Kühn, and K. Rajewsky. 1991. A B cell-deficient mouse by
629 targeted disruption of the membrane exon of the immunoglobulin μ chain
630 gene. *Nature*. 350:423–426. doi:10.1038/350423a0.

631 Kräutler, N.J., D. Suan, D. Butt, K. Bourne, J.R. Hermes, T.D. Chan, C. Sundling, W.
632 Kaplan, P. Schofield, J. Jackson, A. Basten, D. Christ, and R. Brink. 2017.
633 Differentiation of germinal center B cells into plasma cells is initiated by high-
634 affinity antigen and completed by Tfh cells. *Journal of Experimental Medicine*.
635 214:1259–1267. doi:10.1084/jem.20161533.

636 Lefranc, M.-P. 2011. IMGT, the International ImMunoGeneTics Information System.
637 *Cold Spring Harb Protoc*. 2011:pdb.top115. doi:10.1101/pdb.top115.

638 MacLean, A.J., L.P. Deimel, P. Zhou, M.A. ElTanbouly, J. Merkenschlager, V. Ramos,
639 G.S. Santos, T. Hägglöf, C.T. Mayer, B. Hernandez, A. Gazumyan, and M.C.
640 Nussenzweig. 2025. Affinity maturation of antibody responses is mediated by
641 differential plasma cell proliferation. *Science*. 387:413–420.
642 doi:10.1126/science.adr6896.

643 Malladi, S.K., D. Jaiswal, B. Ying, W.B. Alsoussi, T.L. Darling, B. Dadonaite, A. Civljak,
644 S.C. Horvath, J.Q. Zhou, W. Kim, J.S. Turner, A.J. Schmitz, F. Han, S.M.
645 Scheaffer, C.W. Farnsworth, R. Nachbagauer, B. Nestorova, S. Chalkias, M.K.
646 Klebert, D.K. Edwards, R. Paris, B.S. Strnad, W.D. Middleton, J.A. O'Halloran,
647 R.M. Presti, J.D. Bloom, A.C.M. Boon, M.S. Diamond, G. Bajic, and A.H.
648 Ellebedy. 2025. Germinal center–mediated broadening of B cell responses to
649 SARS-CoV-2 booster immunization. *Sci. Immunol.* 10:eadu4107.
650 doi:10.1126/sciimmunol.adu4107.

651 McGuire, A.T., A.M. Dreyer, S. Carbonetti, A. Lippy, J. Glenn, J.F. Scheid, H.
652 Mouquet, and L. Stamatatos. 2014. Antigen modification regulates
653 competition of broad and narrow neutralizing HIV antibodies. *Science*.
654 346:1380–1383. doi:10.1126/science.1259206.

655 McGuire, A.T., M.D. Gray, P. Dosenovic, A.D. Gitlin, N.T. Freund, J. Petersen, C.
656 Correnti, W. Johnsen, R. Kegel, A.B. Stuart, J. Glenn, M.S. Seaman, W.R.
657 Schief, R.K. Strong, M.C. Nussenzweig, and L. Stamatatos. 2016. Specifically

658 modified Env immunogens activate B-cell precursors of broadly neutralizing
659 HIV-1 antibodies in transgenic mice. *Nat Commun*. 7:10618.
660 doi:10.1038/ncomms10618.

661 Merkenschlager, J., R.-M. Berz, V. Ramos, M. Uhlig, A.J. MacLean, C.R. Nowosad,
662 T.Y. Oliveira, and M.C. Nussenzweig. 2023. Continually recruited naïve T cells
663 contribute to the follicular helper and regulatory T cell pools in germinal
664 centers. *Nat Commun*. 14:6944. doi:10.1038/s41467-023-41880-9.

665 Mesin, L., A. Schiepers, J. Ersching, A. Barbulescu, C.B. Cavazzoni, A. Angelini, T.
666 Okada, T. Kurosaki, and G.D. Victora. 2019. Restricted Clonality and Limited
667 Germinal Center Reentry Characterize Memory B Cell Reactivation by
668 Boosting. *Cell*. 0. doi:10.1016/j.cell.2019.11.032.

669 Nussenzweig, M.C., A.C. Shaw, E. Sinn, D.B. Danner, K.L. Holmes, H.C. Morse, and
670 P. Leder. 1987. Allelic Exclusion in Transgenic Mice That Express the
671 Membrane form of Immunoglobulin μ. *Science*. 236:816–819.
672 doi:10.1126/science.3107126.

673 Nutt, S.L., P.D. Hodgkin, D.M. Tarlinton, and L.M. Corcoran. 2015. The generation of
674 antibody-secreting plasma cells. *Nat Rev Immunol*. 15:160–171.
675 doi:10.1038/nri3795.

676 Schaefer-Babajew, D., Z. Wang, F. Muecksch, A. Cho, M. Loewe, M. Cipolla, R.
677 Raspe, B. Johnson, M. Canis, J. DaSilva, V. Ramos, M. Turroja, K.G. Millard,
678 F. Schmidt, L. Witte, J. Dizon, I. Shimeliovich, K.-H. Yao, T.Y. Oliveira, A.
679 Gazumyan, C. Gaebler, P.D. Bieniasz, T. Hatziioannou, M. Caskey, and M.C.
680 Nussenzweig. 2023. Antibody feedback regulates immune memory after
681 SARS-CoV-2 mRNA vaccination. *Nature*. 613:735–742. doi:10.1038/s41586-
682 022-05609-w.

683 Schiepers, A., M.F.L. Van'T Wout, A. Hobbs, L. Mesin, and G.D. Victora. 2024.
684 Opposing effects of pre-existing antibody and memory T cell help on the
685 dynamics of recall germinal centers. *Immunity*. 57:1618-1628.e4.
686 doi:10.1016/j.immuni.2024.05.009.

687 Smith, T. 1909. ACTIVE IMMUNITY PRODUCED BY SO CALLED BALANCED OR
688 NEUTRAL MIXTURES OF DIPHTHERIA TOXIN AND ANTITOXIN. *Journal of*
689 *Experimental Medicine*. 11:241–256. doi:10.1084/jem.11.2.241.

690 Suan, D., C. Sundling, and R. Brink. 2017. Plasma cell and memory B cell
691 differentiation from the germinal center. *Current Opinion in Immunology*.
692 45:97–102. doi:10.1016/j.coi.2017.03.006.

693 Tas, J.M.J., J.-H. Koo, Y.-C. Lin, Z. Xie, J.M. Steichen, A.M. Jackson, B.M. Hauser,
694 X. Wang, C.A. Cottrell, J.L. Torres, J.E. Warner, K.H. Kirsch, S.R. Weldon, B.
695 Groschel, B. Nogal, G. Ozorowski, S. Bangaru, N. Phelps, Y. Adachi, S.
696 Eskandarzadeh, M. Kubitz, D.R. Burton, D. Lingwood, A.G. Schmidt, U. Nair,
697 A.B. Ward, W.R. Schief, and F.D. Batista. 2022. Antibodies from primary

humoral responses modulate the recruitment of naive B cells during secondary responses. *Immunity*. 55:1856-1871.e6. doi:10.1016/j.immuni.2022.07.020.

Todd, D.J., L.J. McHeyzer-Williams, C. Kowal, A.-H. Lee, B.T. Volpe, B. Diamond, M.G. McHeyzer-Williams, and L.H. Glimcher. 2009. XBP1 governs late events in plasma cell differentiation and is not required for antigen-specific memory B cell development. *Journal of Experimental Medicine*. 206:2151–2159. doi:10.1084/jem.20090738.

Viant, C., G.H.J. Weymar, A. Escolano, S. Chen, H. Hartweger, M. Cipolla, A. Gazumyan, and M.C. Nussenzweig. 2020. Antibody Affinity Shapes the Choice between Memory and Germinal Center B Cell Fates. *Cell*. S0092867420313040. doi:10.1016/j.cell.2020.09.063.

Victora, G.D., and M.C. Nussenzweig. 2022. Germinal Centers. *Annu. Rev. Immunol.* 40:413–442. doi:10.1146/annurev-immunol-120419-022408.

Waisman, A., M. Kraus, J. Seagal, S. Ghosh, D. Melamed, J. Song, Y. Sasaki, S. Classen, C. Lutz, F. Brombacher, L. Nitschke, and K. Rajewsky. 2007. IgG1 B cell receptor signaling is inhibited by CD22 and promotes the development of B cells whose survival is less dependent on Igα/β. *The Journal of Experimental Medicine*. 204:747–758. doi:10.1084/jem.20062024.

Wang, Y., J. Shi, J. Yan, Z. Xiao, X. Hou, P. Lu, S. Hou, T. Mao, W. Liu, Y. Ma, L. Zhang, X. Yang, and H. Qi. 2017. Germinal-center development of memory B cells driven by IL-9 from follicular helper T cells. *Nat Immunol*. 18:921–930. doi:10.1038/ni.3788.

Wang, Z., F. Muecksch, R. Raspe, F. Johannsen, M. Turroja, M. Canis, M.A. ElTanbouly, G.S.S. Santos, B. Johnson, V.A. Baharani, R. Patejak, K.-H. Yao, B.J. Chirco, K.G. Millard, I. Shimeliovich, A. Gazumyan, T.Y. Oliveira, P.D. Bieniasz, T. Hatziioannou, M. Caskey, and M.C. Nussenzweig. 2023. Memory B cell development elicited by mRNA booster vaccinations in the elderly. *Journal of Experimental Medicine*. 220:e20230668. doi:10.1084/jem.20230668.

Woodruff, M.C., E.H. Kim, W. Luo, and B. Pulendran. 2018. B Cell Competition for Restricted T Cell Help Suppresses Rare-Epitope Responses. *Cell Reports*. 25:321-327.e3. doi:10.1016/j.celrep.2018.09.029.

Yan, Y., X. Wang, Z. Xie, D.L.V. Bader, R.H. Lim, K.M. Ma, C.A. Cottrell, J.M. Steichen, L. Xu, P.M. Villavicencio, M. Akauliya, J.-H. Koo, J.M. Shen, A. Vernich, O. Kalyuzhniy, J.D. Allen, A.A. Albowaidey, A. Alicea, B. Chen, E. Georgeson, J.R. Ellis-Pugh, N. Alavi, A. Esposito, H. Naili, N. Phelps, B. Kelley, M. Kubitz, Q.A. Phan, A. Liguori, T. Prum, R. Tingle, D. Lu, S. Eskandarzadeh, X. Liu, J.E. Warner, S.R. Weldon, S. Himansu, M. Crispin, U. Nair, S. Liu, W.R. Schief, and F.D. Batista. 2025. Antibody feedback establishes an affinity brake in the germinal center. doi:10.1101/2025.11.13.688298.

Zotos, D., and D.M. Tarlinton. 2012. Determining germinal centre B cell fate. *Trends in Immunology*. 33:281–288. doi:10.1016/j.it.2012.04.003.

742 **Figures and figure legends**

Figure 1

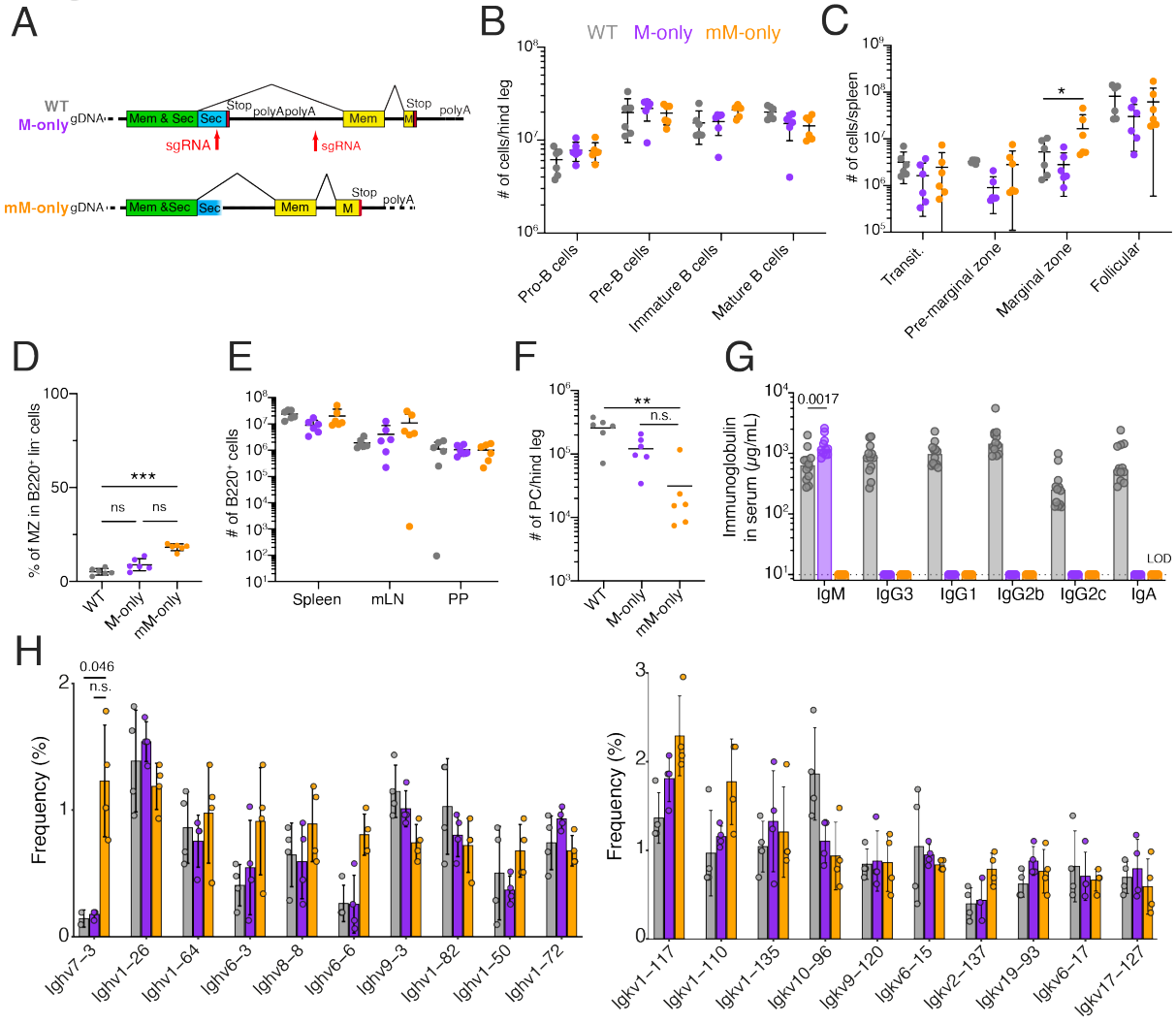

743

744 **Figure 1. B cell development in M-only and mM-only mice.** (**A**) Schematic shows
745 structure of *Ighm* exon 4 in WT, M-only and mM-only mice. (**B**) Number of pro-, pre-
746 , immature and mature B cells in the bone marrow on one leg by flow cytometry.
747 Gating as in Fig. S1 A. (**C**) Number of the splenic B cell subsets by flow cytometry.
748 Gating as in Fig. S1 B. (**D**) Percentage of splenic marginal zone B cells. Gating in Fig.
749 S1B. (**E**) Number of live B cells in spleen, mesenteric lymph node (mLN) and Peyer's
750 Patches (PP) by flow cytometry. Gating in Fig. S1B-D. (**F**) Number of plasma cells in
751 the bone marrow of one leg by flow cytometry. (**G**) ELISA quantification of total IgM,
752 IgG3, IgG1, IgG2b, IgG2c and IgA in the serum of WT, M-only and mM-only mice. (**H**)
753 Bar graph depicting the relative abundance of Ighv (left panel) and Igkv (right panel)
754 gene usage in follicular B cells. Top ten most frequent genes ranked by the mean
755 frequency in mM-only mice are shown. Data was pooled from two independent
756 experiments. Each dot or circle represents a mouse. P-values of non-parametric one-
757 way ANOVA with Tukey's Honest Significance test are shown. All experiments were
758 performed at least twice. **$p < 0.01$ ***$p < 0.001$. Bars indicate mean ± standard
759 deviation (SD).

Figure 2

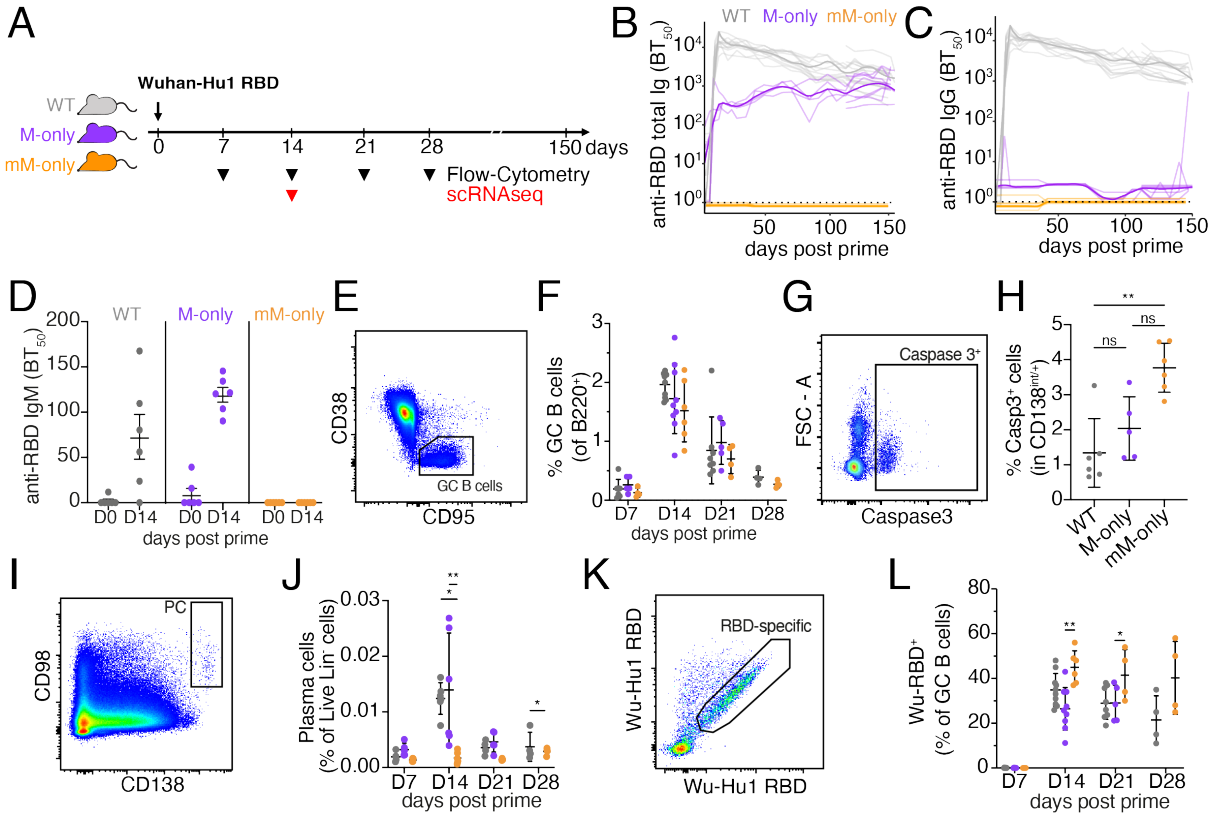
A
Wuhan-Hu1 RBD
WT
M-only
mM-only
0
7
14
21
28
150 days
Flow-Cytometry
scRNAseq
B
WT M-only mM-only
anti-RBD total Ig (BT50)
days post prime
C
anti-RBD IgG (BT50)
days post prime
D
WT M-only mM-only
anti-RBD IgM (BT50)
D0 D14 D0 D14 D0 D14
days post prime
E
CD38
GC B cells
CD95
F
% GC B cells (of B220+)
D7 D14 D21 D28
days post prime
G
Caspase 3+
FSC - A
Caspase3
H
% Casp3+ cells (in CD138int/+)
ns
ns
WT
M-only
mM-only
I
PC
CD98
CD138
J
Plasma cells (% of Live Lin- cells)
D7 D14 D21 D28
days post prime
K
RBD-specific
Wu-Hu1 RBD
Wu-Hu1 RBD
L
Wu-RBD+ (% of GC B cells)
D7 D14 D21 D28
days post prime

760

761 **Figure 2. Primary vaccine responses.** (**A**) Diagram of the experimental protocol. (**B**)
762 ELISA quantification of anti-RBD antibodies in the serum measured every 3 to 5 days
763 between D0 and D150. (**C**) As in (B) for IgG anti-RBD antibodies in the serum. Thin
764 lines (in B and C) represent single mice, bold lines represent group mean. (**D**) Serum
765 anti-RBD IgM ELISA 0 or 14 after immunization. (**E**) Flow cytometric gating for $CD38^{-}$
766 $CD95^{+}$ GC B cells. Pre-gated on $B220^{+}$ cells in draining lymph nodes (dLN). (**F**)
767 Quantification of GC B cells from (E) at the indicated time points after immunization.
768 (**G**) Flow cytometry gating for $Caspase3^{+}$ cells among $CD138^{int/+}$ live $Dump^{-}$ cells. (**H**)
769 Quantification of (G) among $CD138^{int/+}$ live $Dump^{-}$ cells in dLN 14 days after
770 immunization. (**I**) Flow cytometric gating for $CD98^{+}$ $CD138^{+}$ PC pre-gated on live
771 $Dump^{-}$ cells in the dLN. (**J**) Quantification of (I) at the indicated times after
772 immunization. (**K**) Flow cytometric gating of RBD^{+} cells among GC B cells in the
773 draining LNs. Pre-gated for GC as in (E). (**L**) Quantification of (K) at the indicated time
774 points after immunization. Each dot in all dot plots represents one mouse. P-values
775 of non-parametric one-way ANOVA are shown. All experiments were performed at
776 least twice. Bars in (D, F, H, J and L) indicate mean ± SD. $^{**}p < 0.01$, $^{*}p < 0.05$.

Figure 3

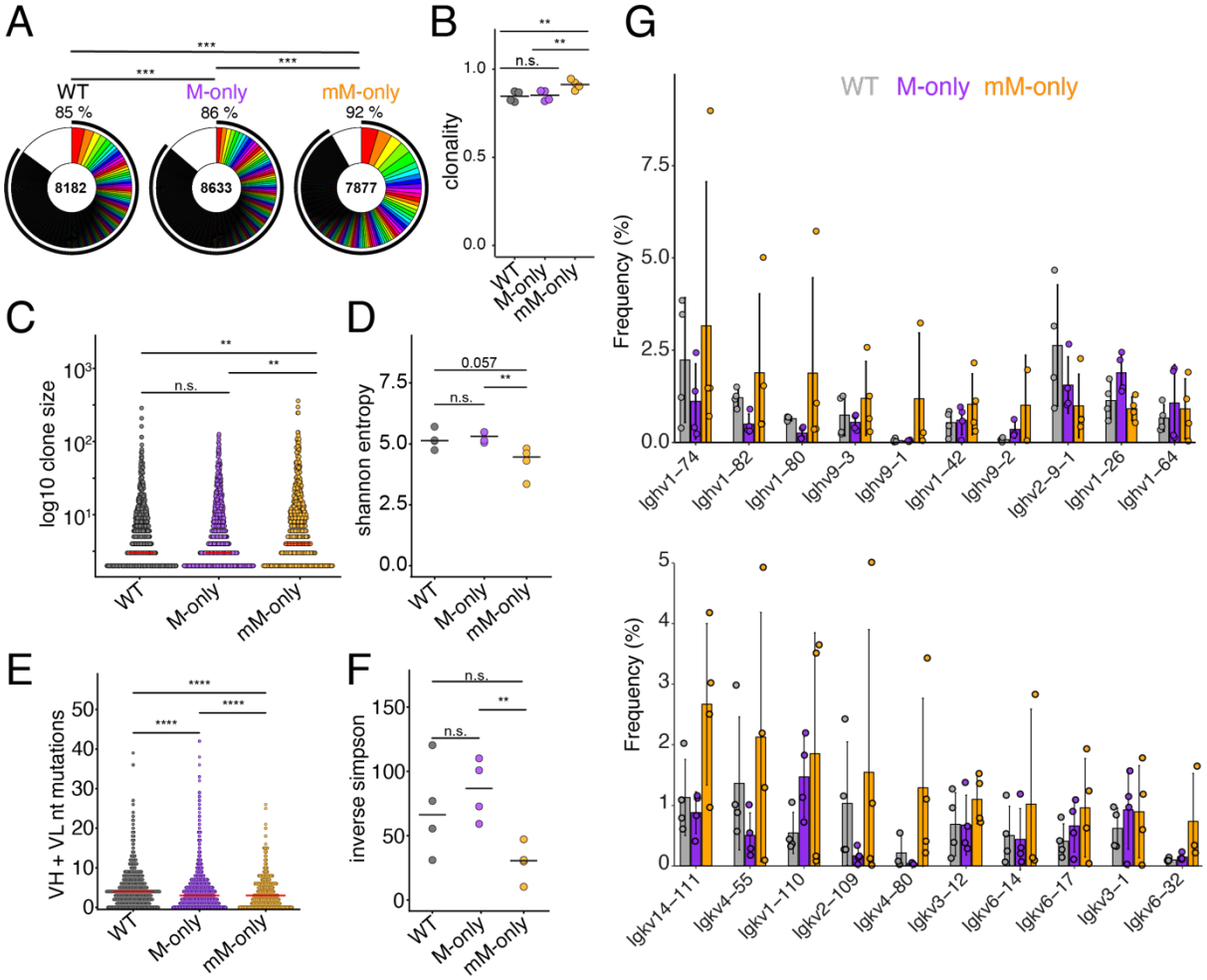
A
WT
85 %
8182
M-only
86 %
8633
mM-only
92 %
7877
B
clonality
n.s.
C
log10 clone size
n.s.
D
shannon entropy
0.057
n.s.
E
VH + VL nt mutations
F
inverse simpson
n.s.
G
WT M-only mM-only
Frequency (%)
Ighv1–74
Ighv1–82
Ighv1–80
Ighv9–3
Ighv9–1
Ighv1–42
Ighv9–2
Ighv2–9–1
Ighv1–26
Ighv1–64
Igkv14–111
Igkv4–55
Igkv1–110
Igkv2–109
Igkv4–80
Igkv3–12
Igkv6–14
Igkv6–17
Igkv3–1
Igkv6–32

777

Figure 3. Primary GC antibody sequences. (**A**) Pie charts depicting the distribution of antibody sequences pooled from 4 mice/genotype obtained 14 days after prime immunization from GC B cells. Inner circle numbers indicate the number of sequences analyzed for each genotype. White section indicates sequences non-expanded sequences, colored or black pie slices are proportional to the number of clonally related sequences. The outlined black line indicates the percentages of cells in a clonal family. (**B**) Dot plot illustrating the percentage of clonally expanded sequences within each mouse. Each dots indicates one mouse. Bars indicate mean. (**C**) Dot plot showing clonotypes size distribution. Bars indicate median. Each dot indicates a clone. (**D**) Dot plot showing Shannon entropy scores for the sequences depicted in (A) within each mouse. Bars indicate median. (**E**) Dot plot showing combined VH + VL gene nucleotide mutations among sequences show in (A). Each dot indicates an antibody VH+VL pair. Bars indicate median. (**F**) Dot plot depicting inverse Simpson index for sequences shown in (A) for each mouse. Each dots indicates one mouse. Bars indicate median. (**G**) Bar graphs showing the relative abundance of mouse Ighv and Igkv gene usage among sequences shown in (A). Top ten most frequent genes ranked by the mean frequency in mM-only mice are shown. Bars indicate mean ± SD. Statistics in (A) indicate chi-squared test with Monte Carlo p-value simulation, p-values were subsequently corrected using the Benjamini-Hochberg (BH) procedure. Statistics in (B)-(F) indicate two-sided Mann-Whitney U test. ****$p<0.0001$, ***$p<0.001$,**$p<0.01$, *$p<0.05$.

Figure 4

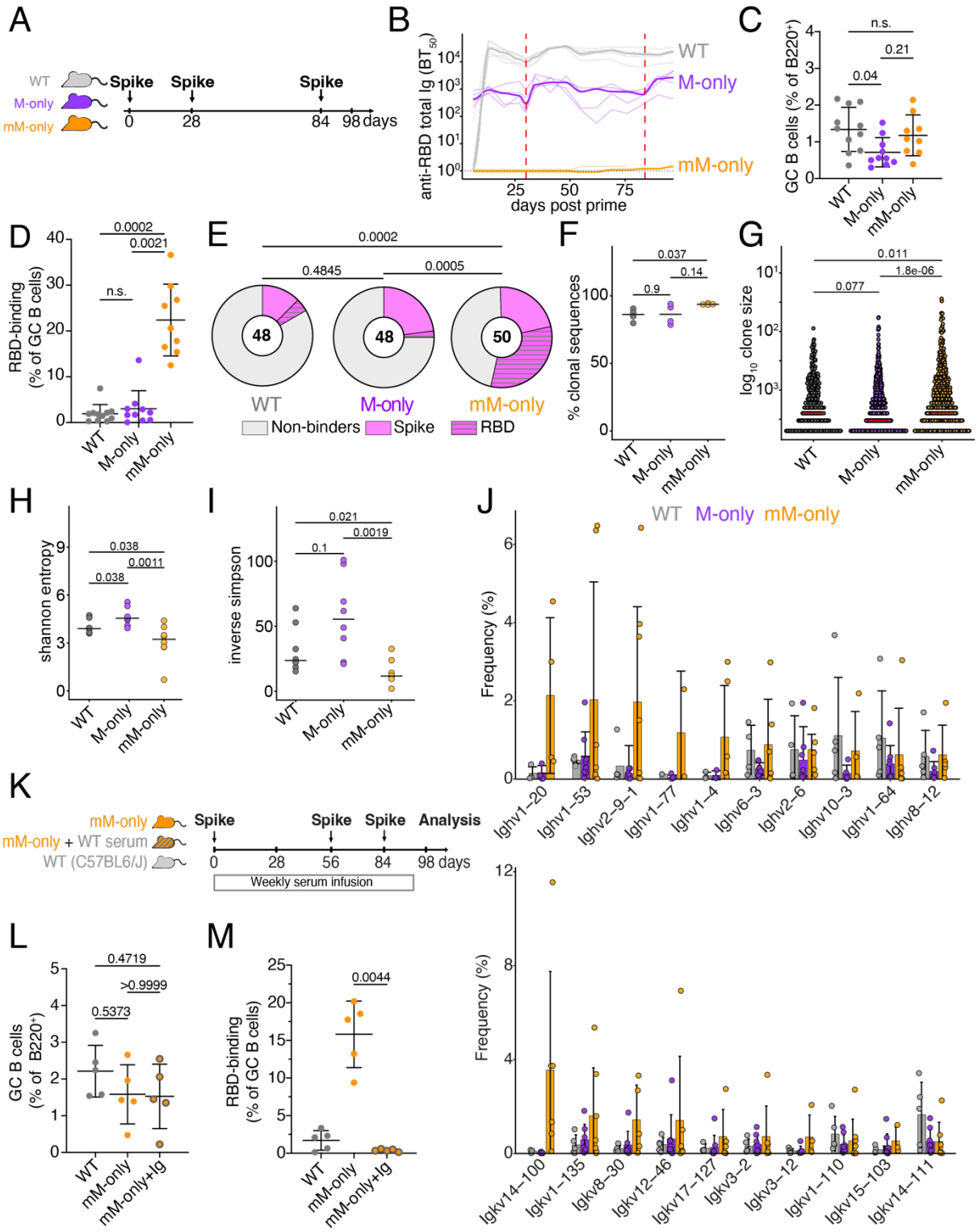
A
WT
M-only
mM-only
Spike
Spike
Spike
0
28
84
98 days
B
anti-RBD total Ig (BT50)
WT
M-only
mM-only
25
50
75
days post prime
C
GC B cells (% of B220+)
n.s.
0.21
0.04
WT
M-only
mM-only
D
RBD-binding (% of GC B cells)
0.0002
0.0021
n.s.
WT
M-only
mM-only
E
0.0002
0.4845
0.0005
48
48
50
WT
M-only
mM-only
Non-binders
Spike
RBD
F
% clonal sequences
0.037
0.14
0.9
WT
M-only
mM-only
G
log10 clone size
0.011
1.8e-06
0.077
WT
M-only
mM-only
H
shannon entropy
0.038
0.0011
0.038
WT
M-only
mM-only
I
inverse simpson
0.021
0.0019
0.1
WT
M-only
mM-only
J
WT
M-only
mM-only
Frequency (%)
Ighv1–20
Ighv1–53
Ighv2–9–1
Ighv1–77
Ighv1–4
Ighv6–3
Ighv2–6
Ighv10–3
Ighv1–64
Ighv8–12
K
mM-only
mM-only + WT serum
WT (C57BL6/J)
Spike
Spike
Spike
Analysis
0
28
56
84
98 days
Weekly serum infusion
L
GC B cells (% of B220+)
0.4719
>0.9999
0.5373
WT
mM-only
mM-only+Ig
M
RBD-binding (% of GC B cells)
0.0044
WT
mM-only
mM-only+Ig
Frequency (%)
Igkv14–100
Igkv1–135
Igkv8–30
Igkv12–46
Igkv17–127
Igkv3–2
Igkv3–12
Igkv1–110
Igkv15–103
Igkv14–111

799

800 **Figure 4. Prime boost vaccination.** (**A**) Diagram of the experimental protocol for (A)
801 to (J). (**B**) ELISA quantification of total anti-RBD antibodies in the serum measured
802 weekly from D6 to D97 after prime immunization. Thin lines represent single mice,
803 bold line indicates group mean. Dashed red lines indicate booster immunizations. (**C**)
804 Percentage of GC B cells among $B220^+$ B cells in the draining LN at D98. Gating as
805 in (Fig. 2 E). (**D**) Percentage of RBD-binding GC B cells in the draining LN at D98.
806 Each dot represents one mouse. Gating as in (Fig. 2 K). Each dot represents one
807 mouse. Bars indicate mean ± SD (**E**) Pie charts depicting the distribution of RBD-
808 binding, Spike-binding or non-binding recombinant antibodies cloned from the
809 largest expanded clones of 4 mice/group of GC B cells on D98 from draining LNs.
810 $BT_{50} < 10$ μg/mL considered binders. Inner circle numbers indicate the number of
811 recombinant antibodies analyzed. (**F**) Dot plot showing the percentage of clonal
812 sequences from GC B cells on Day 98. Each dot represents one mouse. Bars indicate
813 median. (**G**) Number of mutations in GC B cells on D98. Each dot represents one
814 clone. Bars indicate median. (**H**) Dot plot depicting the Shannon entropy for
815 sequences from (F). (**I**) Dot plots depicting the inverse Simpson index for sequences
816 from (F). Each dot represents one mouse. Bars indicate median. (**J**) Bar graphs
817 showing the relative abundance of mouse Ighv and Igkv gene usage among
818 sequences from (F). Top ten most frequent genes ranked by the mean frequency in
819 mM-only mice are shown. Bars indicate mean ± SD. (**K**) Diagram of the experimental
820 protocol for (L) and (M). (**L**) Percentage of GC B cells among $B220^+$ B cells in the
821 draining LN on day 98. Each dot represents one mouse. Gating as in (Fig. 2 E). Bars
822 indicate mean ± SD (**M**) Percentage of RBD-binding GC B cells. Each dot represents
823 one mouse. Gating as in (Fig. 2K). Bars indicate mean ± SD. Statistics in (C), (D), (J),

824 (L) and (M) indicate non-parametric, one-way ANOVA p-values. Statistics in (E)-(I)
825 indicate two-sided Mann-Whitney U test. ****$p<0.0001$, ***$p<0.001$,**$p<0.01$,
826 *$p<0.05$. All flow cytometry experiments are from at least 2 independent experiments.

Figure 5

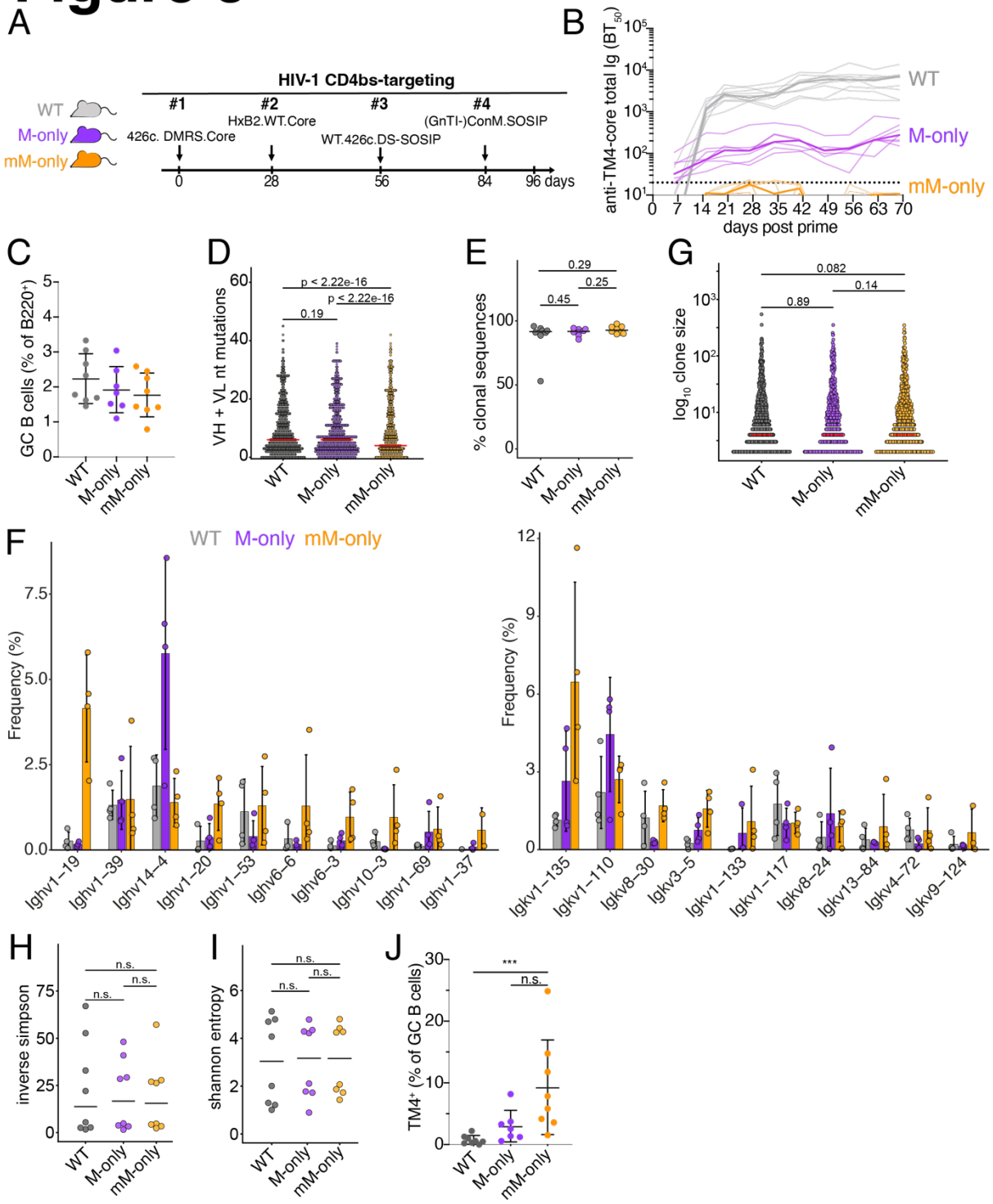
A
HIV-1 CD4bs-targeting
WT
M-only
mM-only
#1
426c. DMRS.Core
#2
HxB2.WT.Core
#3
WT.426c.DS-SOSIP
#4
(GnTI-)ConM.SOSIP
0
28
56
84
96 days
B
anti-TM4-core total Ig (BT50)
days post prime
WT
M-only
mM-only
C
GC B cells (% of B220+)
D
VH + VL nt mutations
p < 2.22e-16
p < 2.22e-16
0.19
E
% clonal sequences
0.29
0.25
0.45
G
log10 clone size
0.082
0.14
0.89
F
Frequency (%)
Ighv1-19
Ighv1-39
Ighv14-4
Ighv1-20
Ighv1-53
Ighv6-6
Ighv6-3
Ighv10-3
Ighv1-69
Ighv1-37
Igkv1-135
Igkv1-110
Igkv8-30
Igkv3-5
Igkv1-133
Igkv1-117
Igkv8-24
Igkv13-84
Igkv4-72
Igkv9-124
H
inverse simpson
n.s.
I
shannon entropy
n.s.
J
TM4+ (% of GC B cells)
***
n.s.

827

828 **Figure 5. Sequential immunization with an HIV-1 antigen series.** (**A**) Diagram of
829 the experimental protocol. (**B**) ELISA quantification of total anti-TM4-core serum
830 antibodies measured weekly from day 6 to 69. Thin lines represent single mice, bold
831 lines represent group mean. (**C**) Percentage of GC B cells among B220^{+} B cells in the
832 draining LN on day 96. Gating as in (Fig. 2 E). Bars indicate mean ± SD. (**D**) Dot plot
833 showing combined VH + VL gene nucleotide mutations among GC B cells sequences
834 on day 96. Each dot indicates an antibody VH+VL pair. Bars indicate median. (**E**)
835 Proportions of clonal sequences within each mouse at day 96. Each dot indicates
836 sequences from one mouse. Bars indicate median. (**F**) Bar graph showing the relative
837 abundance of mouse Ighv left panel) and Igkv (right panel) gene usage in GC B cells
838 on day 96. Top ten most frequent genes ranked by the mean frequency in mM-only
839 mice are shown. Bars indicate mean ± SD (**G**) Dot plot depicting the percentage of
840 clonal sequences from GC B cells on day 96. Each dot indicates a clone. Bars indicate
841 median. (**H**) Dot plot depicting Inversed Simpson index of antibody sequences from
842 day 96 GC B cells. Each dots represents one mouse. Bars indicate median. (**I**) Dot
843 plot showing the Shannon entropy index form day 96 GC B cells. Each dots
844 represents one mouse. Bars indicate median. (**J**) Percentages of TM4-binding GC B
845 cells. p-values of non-parametric one-way ANOVA indicated. ***$p < 0.001$.

Figure S1

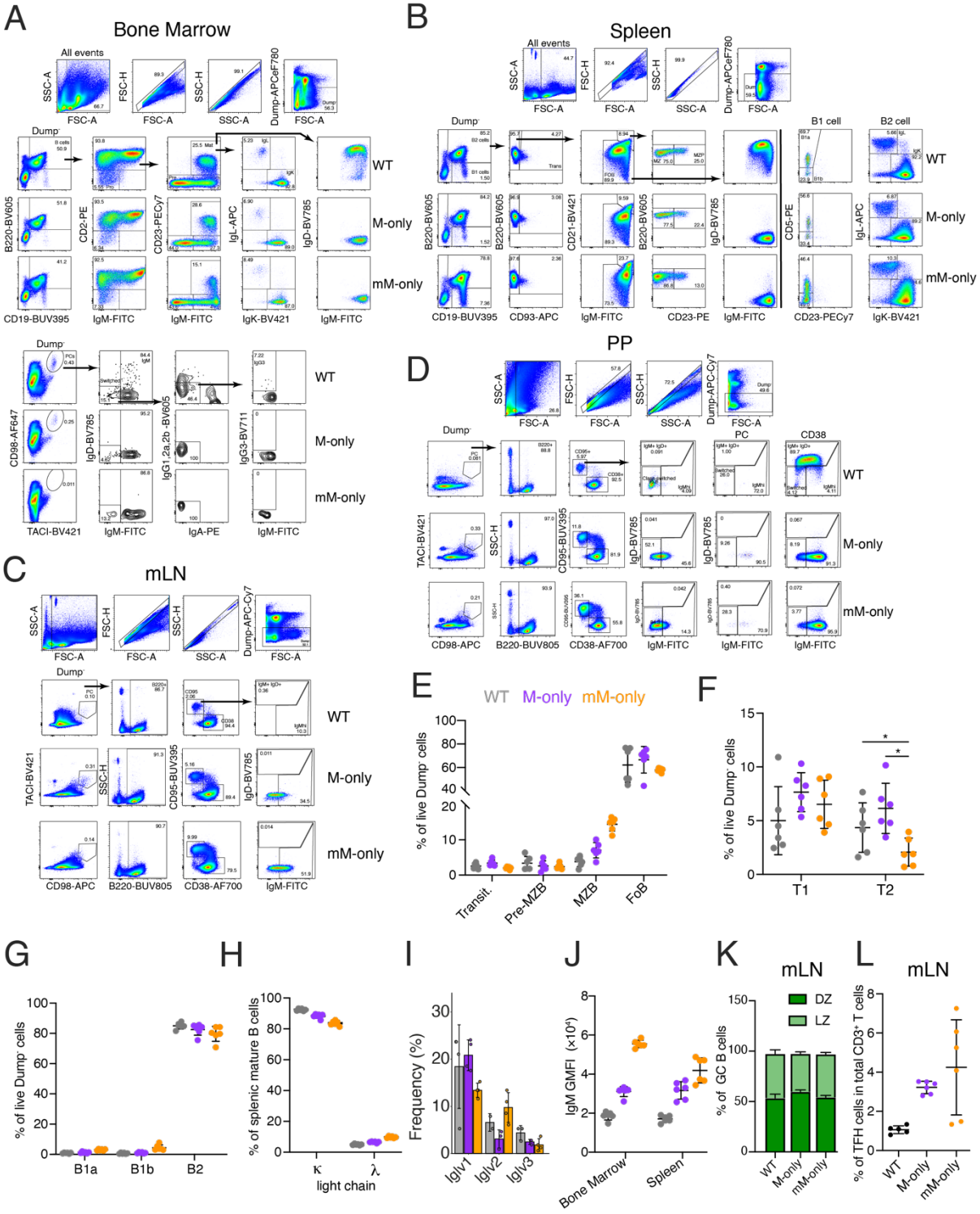

846

847 **Figure S1. Analysis of M-only and mM-only mouse strains.** Related to Fig. 1. (**A**)
848 Flow cytometric gating strategy in the bone marrow. All stainings were cell surface
849 and not intracellular stainings. (**B**) Flow cytometric gating strategy in the spleen. (**C**)
850 Flow cytometric gating strategy in the mesenteric LN (mLN). (**D**) Flow cytometric
851 gating strategy in the Peyer's patches (PP). (**E**) Percentages of splenic, transitional
852 (Transit), pre-marginal zone (Pre-MZB), marginal zone (MZB) , and follicular (FoB) B
853 cells among live $Dump^-$ cells. (**F**) Percentages of transitional T1 and T2 B cells in live
854 $Dump^-$ cells. (**G**) Percentages of splenic B1a, B1b and B2 cells among live $Dump^-$
855 cells. (**H**) Percentages of splenic κ or λ light chain bearing mature B cells. (**I**) Bar
856 graphs showing Iglv gene usage in follicular B cells. Top ten most frequent genes
857 ranked by the mean frequency in mM-only mice are shown. (**J**) Geometric mean
858 fluorescence intensity (GMFI) of IgM-FITC in the bone marrow mature B cells and
859 splenic follicular B cells. (**K**) Proportions of DZ and LZ B cells in mesenteric lymph
860 nodes at steady state. (**L**) Proportions of T follicular helper cells in mLN at steady
861 state in total $CD3^+$ T cells. Each dot represents a single mouse. Bars indicate mean ±
862 SD.

Figure S2

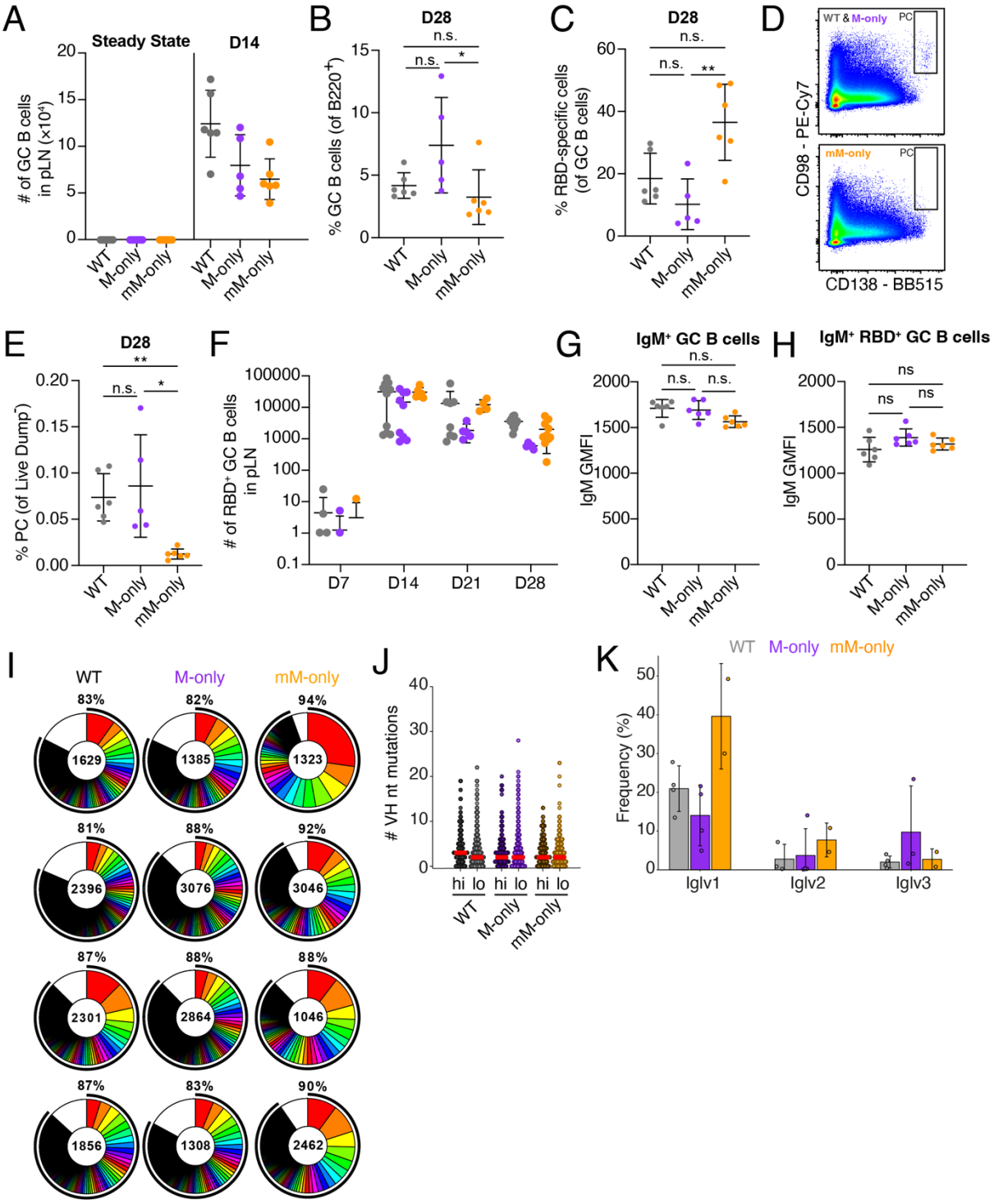

863

864 **Figure S2. Prime immunization with RBD**. Related to Fig. 2 and 3. (**A**) Absolute
865 numbers of GC B cells in draining LN at steady state (left) and 14 days after RBD
866 immunization (right). (**B**) Proportions of GC B cells in B220$^+$ B cells at day 28 after
867 immunization. (**C**) Proportions of RBD-specific cells in GC B cells at day 28 after
868 immunization. (**D**) Flow cytometric gating strategy for PC. (**E**) Proportions of PC in live
869 dump$^-$ cells. (**F**) Numbers of RBD$^+$ GC B cells at D7, D14, D21 and D28 after RBD
870 immunization. (**G**) IgM geometric mean fluorescence intensity (GMFI) in CD95$^+$ B220$^+$
871 GC B cells. (**H**) IgM GMFI in RBD-specific CD95$^+$ B220$^+$ GC B cells. (**I**) Pie charts
872 depicting the distribution of antibody sequences obtained 14 days after prime
873 immunization from GC B cells from 4 mice/genotype. Inner circle numbers indicate
874 the number of sequences analyzed for each mouse. White section indicates non-
875 expanded sequences, colored or black pie slices are proportional to the number of
876 clonally related sequences. The outlined black line indicates the percentages of cells
877 in a clonal family. (**J**) Iglv gene usage frequency in genotypes. VH genes split by the
878 mean frequency in mM-only are shown. Top 10 highest frequency (hi) and remaining
879 low frequency VH genes (lo) are plotted. Each dots represents a VH gene. Bars
880 indicate median. (**K**) Dot plot showing the number of VH nucleotide somatic
881 hypermutations in sequences from top 10 most frequent V genes in mM-only mice
882 from Fig. 5 F (Hi) compared with sequences from all remaining low-frequency V
883 genes. Each dot indicates VH sequence from one cell. Bars indicate median. Each
884 dot represents a single mouse. Bars indicate mean ± SD. *$p<0.05$, **$p<0.01$ in one-
885 way ANOVA.

Figure S3

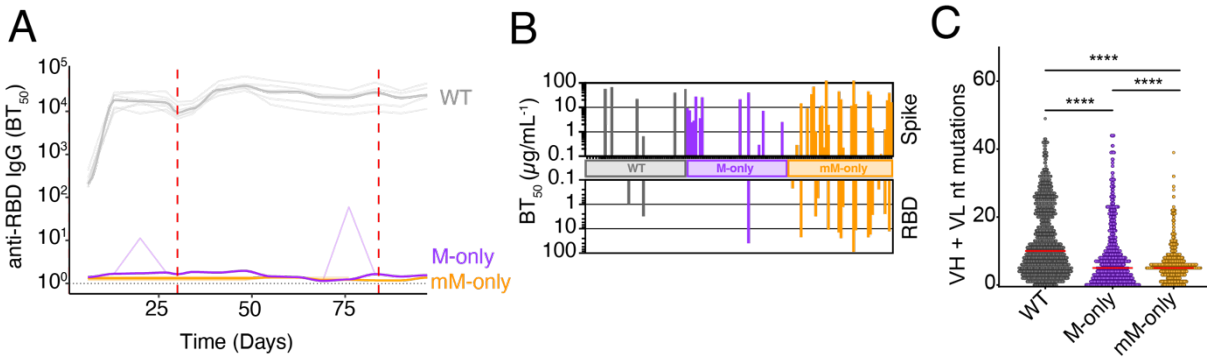

886

887 **Figure S3. Analysis of anti-Spike prime boost responses.** Related to Fig. 4. (**A**)
888 ELISA quantification of anti-RBD IgG antibodies in the serum of mice from Fig. 4
889 measured weekly from day 6 to day 97. Thin lines represent single mice, bold lines
890 represent group mean. (**B**) Bar graph of recombinant antibodies binding to Spike (top)
891 or RBD (bottom) protein. Each bar represents one antibody. (**C**) Dot plot depicting
892 somatic hypermutations in GC B cells on day 98 from Fig. 4. Each dot indicates one
893 sequence. Bars indicate median. P-value of two-sided Mann-Whitney U test
894 indicated. ****$p<0.0001$

Figure S4

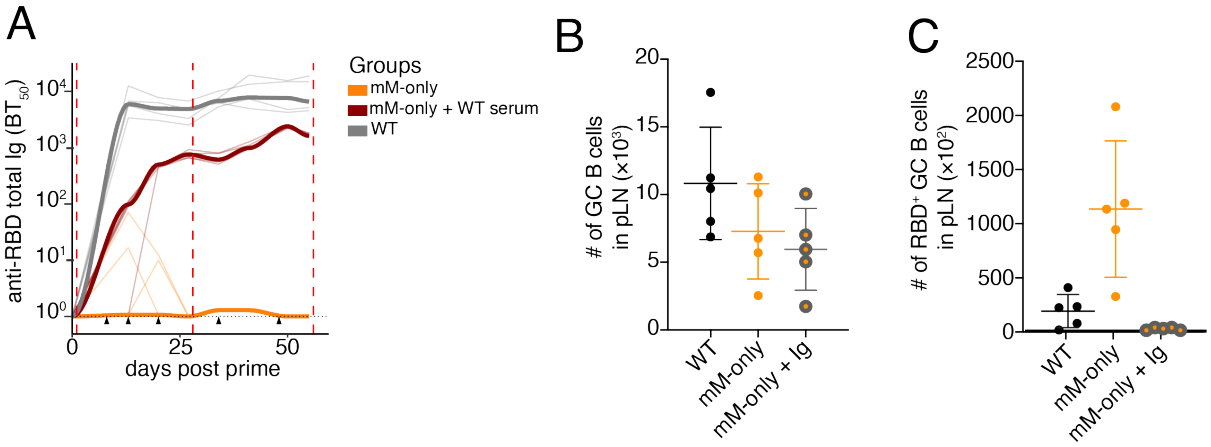

895

896 **Figure S4. Analysis of serum transfer experiment.** Related to Fig. 5. (**A**) ELISA
897 quantification of anti-RBD total Ig antibodies in the serum measured weekly from day
898 0 to day 55. Red dashed lines indicate immunizations, black triangles indicate serum
899 transfer. Thin lines indicate individual mice, bold lines indicate group mean. (**B**)
900 Number of GC B cells in dLN. (**C**) Number of RBD-specific GC B cells in dLN. Each
901 dot represents a single mouse, bars indicate mean ± SD.

Figure S5

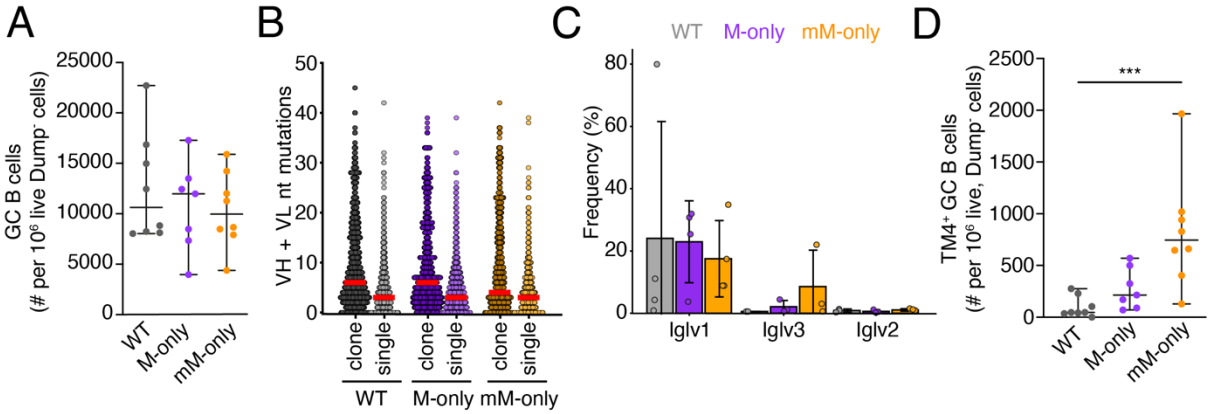

902

903 **Figure S5. Analysis of anti-HIV-1 sequential immunization.** Related to Fig. 5. (**A**)
904 Number of GC B cells in draining lymph nodes after sequential immunizations on day
905 96. (**B**) Dot plot showing combined VH + VL gene nucleotide mutations among
906 clonally expanded sequences compared with non-expanded sequences (singlets).
907 Each dot indicates an antibody VH+VL pair. Bars indicate median. (**C**) Bar graphs
908 showing Iglv gene usage in GC B cells. Top ten most frequent genes ranked by the
909 mean frequency in mM-only mice are shown. (**D**) Number of TM4-binding GC B cells
910 in sequentially immunized mice on day 96 in draining LNs. Each dot represents a
911 single mouse, bars indicate mean ± SD unless otherwise indicated. ***$p<0.001$ non-
912 parametric one-way ANOVA p-values are shown.
913
914
915
916 **Table S1. Recombinant antibody sequences and binding data.** Related to Fig. 4.
917
918 **Table S2. Flow Cytometric reagents.**

Acknowledgements

We thank Kristie Gordon and Jean-Philip Truman for assistance with cell sorting, Thomas Eisenreich for help with mouse colony management and technical help; Masa Jankovic and Tacio A. Waldetario for laboratory support; and all members of the Nussenzweig laboratory and HIVRAD P01 (2P01AI100148) collaborators for helpful discussions.

Funding

This work was supported in part by by the Human Immunome Project and Michelson Medical Research Foundation's Michelson Prize: Next Generation Grant to D.S.B.; NIH grants 2P01AI100148-11 (HIVRAD) to M.C.N; UM1AI191237 (INSPIRE) to H.H. and M.C.N., 1UM1AI144462-01 (CHAVD) to M.C.N. and the Stavros Niarchos Foundation Institute for Global Infectious Disease Research. D.S.B. was supported in part by the National Center for Advancing Translational Sciences (NIH Clinical and Translational Science Award program, grant UL1-TR001866) and the Shapiro–Silverberg Fund for the Advancement of Translational Research. M.C.N. is a Howard Hughes Medical Institute investigator.

Author contributions

D.S.B., H.H. and M.C.N conceived the study. D.S.B and H.H. generated the novel mouse strains described in this manuscript. D.S.B., L.B. and H.H. designed and performed the experiments and interpreted data. G.S.S.S. performed bioinformatic analysis. C.R., L.D., M.A.E., D.G., G.L.D.R., and C.U. assisted and performed experiments. K.H.Y. assisted with mouse experiments and husbandry; B.H. and A.G.

943 produced recombinant proteins and antibodies. P.A. and L.S. provided HIV reagents.
944 M.C.N. supervised the study, designed experiments and interpreted data. D.S.B.,
945 L.B., H.H. and M.C.N. wrote the manuscript. All authors edited the manuscript.
946
947 **Competing interests**
948 M.C.N. is on the scientific advisory board of Celldex Therapeutics. All other authors
949 declare that they have no competing interests.
950
951 **Data and materials availability**
952 All data needed to evaluate the conclusions in the paper are available in the main text
953 and supplementary materials. Reagents, including mouse strains, are available from
954 H.H. and M.C.N. under a material transfer agreement with The Rockefeller University
955 under reasonable request.
956
957 **License information**
958 This article is subject to HHMI's Open Access to Publications policy. HHMI lab heads
959 have previously granted a nonexclusive CC BY 4.0 license to the public and a
960 sublicensable license to HHMI in their research articles. Pursuant to those licenses,
961 the Author Accepted Manuscript (AAM) of this article can be made freely available
962 under a CC BY 4.0 license immediately upon publication.